A Numerical Study of the Circulation of the Bering Sea Basin and Exchange with the North Pacific Ocean*

JAMES E. OVERLAND

Pacific Marine Environmental Laboratory/NOAA, Seattle, Washington

MICHAEL C. SPILLANE

Joint Institute for the Study of Atmosphere and Ocean, University of Washington, Seattle, Washington

HARLEY E. HURLBURT

Naval Research Laboratory, Stennis Space Center, Mississippi

ALAN J. WALLCRAFT

Planning Systems Incorporated, Slidell, Louisiana

(Manuscript received 28 July 1992, in final form 25 May 1993)

ABSTRACT

A limited-area, primitive equation, three-layer hydrodynamic model, with realistic coastlines and bathymetry and 1/8° resolution, is used to investigate the circulation of the Bering Sea basin and the adjacent North Pacific Ocean. The westward flowing Alaskan Stream to the south of the Aleutian Island chain is specified as a boundary condition at inflow and outflow ports with a constant throughput of 15 Sv (Sv $\equiv 1 \times 10^6$ m^3 s^{-1}). Atmospheric forcing is based on the Hellerman and Rosenstein monthly climatological wind field. The model is spun up over 50 years and the statistics of the final decade are described. The general features of the model circulation as discussed below are consistent with available hydrographic and buoy drift observations. The model Alaskan Stream separates from the Aleutian Island chain near 175°E; beyond this point there is strong interannual variability associated with meandering and occasional eddy shedding along the northern arm of the western subarctic gyre. There is a generally cyclonic, but spatially complex and nonstationary, circulation within the Bering Sea basin, fed by inflow through the Aleutian passes; outflow is confined to Kamchatka Strait and varies seasonally, between 8.5 Sv in summer and 13 Sv in winter. A region of intense eddy activity lies west-northwest of Bowers Ridge. The model predicts seasonal reversals in the Bering slope current that are not clearly evident in the temporally sparse observational database. The numerical study demonstrates that flow instabilities contribute to substantial interannual variability in the circulation of the Bering Sea and adjacent northwest Pacific Ocean.

1. Introduction

There have been few modern measurements or analyses of the circulation over the deep Bering Sea (Fig. 1). Observations of circulation in the Bering Sea and transport through the Aleutian passes made in the 1930s (Barnes and Thompson 1938) and prior to the early 1970s (Reid 1973; Sayles et al. 1979) were in the form of isolated hydrographic surveys and anchor stations over at most several days. A most striking feature of the previous analyses is the difference between the proposed circulation patterns for the western Bering Sea. For example, Hughes et al. (1974) emphasized drift measurements with rather uniform flow while Takenouti and Ohtani (1974) emphasize eddylike features in dynamic topography. There was general agreement that the inflow to the Bering Sea is mainly through the western Aleutian passes, primarily Near Strait, and that the outflow is in the far west as the Kamchatka Current. However, there is much uncertainty as to the temporal and spatial variability of flow, even for one pass (Favorite 1974). A recent year-long mooring in Amchitka Pass (Reed 1990) gives an annual northward transport of 2 Sv (Sv $\equiv 10^6$ m^3 s^{-1}) but with southward transport between August and October. Solomon and Ahlnäs (1978), using early satellite imagery, noted eddylike activity in the Kamchatka Current and called

* Contribution Number 1339 from NOAA/Pacific Marine Environmental Laboratories. Contribution Number 182 to JISAO, University of Washington. Contribution Number JA323:091:92 to the Naval Research Laboratory.

Corresponding author address: Dr. James E. Overland, NOAA/PMEL/R/PM, Bin C15700, Bldg. 3, 7600 Sand Point Way NE, Seattle, WA 98115-0070.

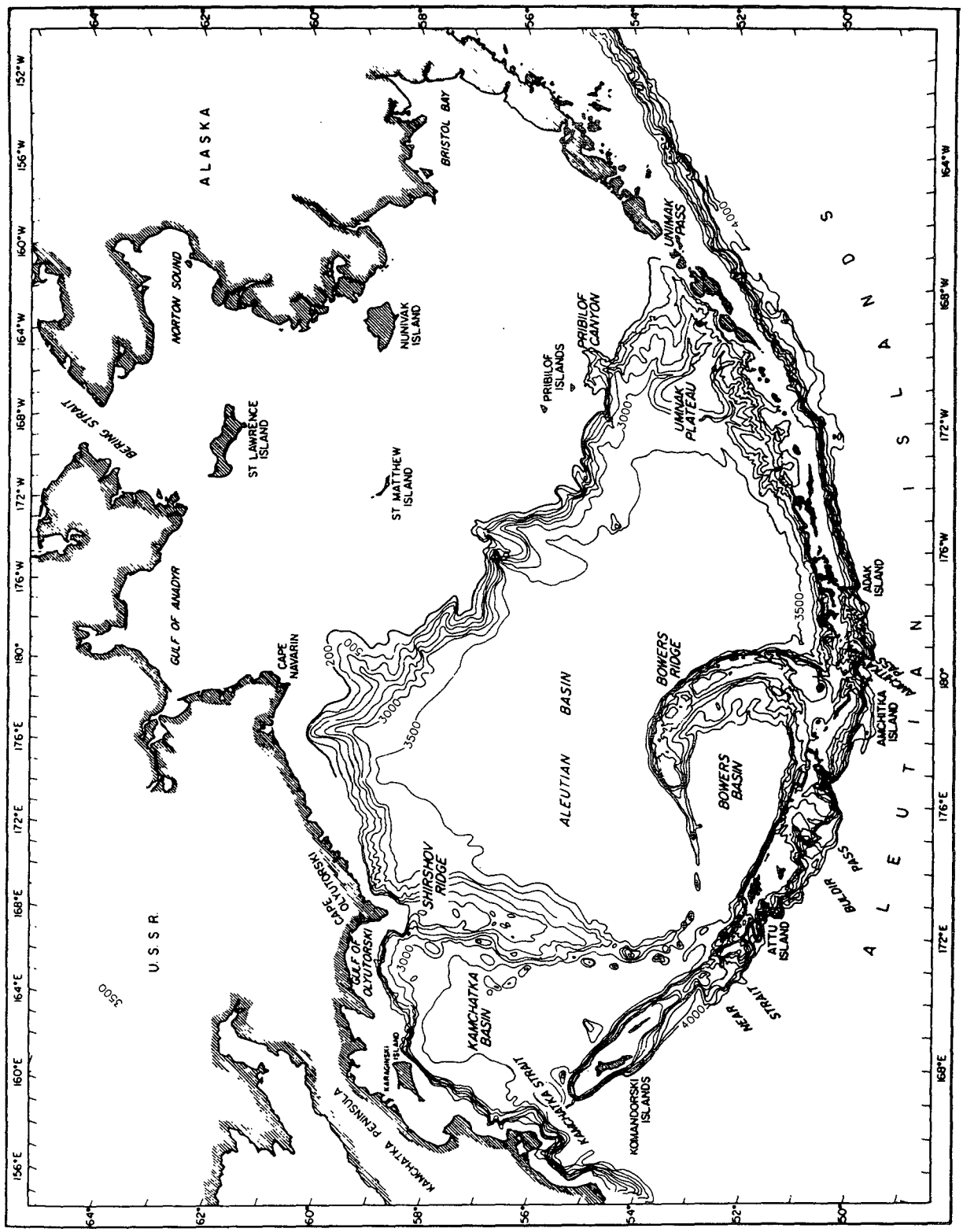

FIG. 1. Chart of the Bering Sea shelf and basin. The contour interval is 500 m except between Cape Navarin and Unimak Pass where the 200-m isobath is shown.

TABLE 1. Definition of variables and constants.

h_k	kth layer thickness
$\mathbf{v}_k$	kth layer velocity
$\mathbf{V}_k$	$h_k\mathbf{v}_k$
H_k	kth layer rest thickness, $k = 1 \cdots n$
H_n	$D(x, y) - \sum_{l=1}^{n-1} H_l$
$D(x, y)$	total depth of ocean at rest
f	Coriolis parameter
A_H	coefficient of horizontal eddy viscosity
ρ_k	kth layer density, constant in space and time
G_{kl}	$\begin{cases} g & \text{for } l \leqslant k \\ g - g(\rho_l - \rho_k)/\rho_0 & \text{for } l > k \end{cases}$
$\vec{\tau}_k$	$\begin{cases} \vec{\tau}_w & \text{for } k = 0 \\ C_k\rho_0\lvert\mathbf{v}_k - \mathbf{v}_{k+1}\rvert(\mathbf{v}_k - \mathbf{v}_{k+1}) & k = 1, \cdots, n-1 \\ C_b\rho_0\lvert\mathbf{v}_n\rvert\mathbf{v}_n & \text{for } k = n \end{cases}$
$\vec{\tau}_w$	wind stress
C_k	coefficient of interfacial friction
C_b	coefficient of bottom friction
ω_k	$\begin{cases} 0 & \text{for } k = 0, k = n \\ \max(0, \omega_k^+) - \max(0, \omega_k^-) - h_k\hat{\omega}_k & \text{for } k = 1, \cdots, n-1 \end{cases}$
ω_k^+	$\frac{1}{4}\tilde{\omega}_k[h_k^+/h_k - 1]$
ω_k^-	$\frac{1}{4}\tilde{\omega}_k[h_k^-/(h_k^- + h_k^+ - h_k) - 1]$
$\hat{\omega}_k$	$\iint [\max(0, \omega_k^+) - \max(0, \omega_k^-)]/\iint H_k$
$\tilde{\omega}_k$	kth interface reference vertical mixing velocity
h_k^+	kth layer thickness at which entrainment starts
h_k^-	kth layer thickness at which detrainment starts

into question previous conclusions based on hydrographic surveys due to the exceptionally high space and time variability in the computed geostrophic transports. These results indicate a need for new approaches to clarify the nature of the net circulation in the North Pacific and Bering Sea and its seasonal and interannual variability.

Oceanographic research in the Bering Sea has often been in response to interest in fisheries. This was the case in 1935 (Barnes and Thompson 1938), the period 1955–1970, and the present (NOAA 1991) where extensive observational efforts are under way as part of Bering Sea FOCI (Fisheries–Oceanography Coordinated Investigations), a component of NOAA's Coastal Ocean Program. Reed et al. (1992) describe a cruise to the western Bering Sea during 1991 in which CTD and ADCP (Acoustic Doppler Current Profiler) measurements were collected and satellite-tracked buoys and year-long moorings were deployed. The buoy releases continue a series begun in 1986, and have been used by Stabeno and Reed (1994) to derive a composite circulation chart for the Bering Sea basin and adjacent North Pacific Ocean. The trajectory of a single buoy, released serendipitously in the Bering Sea in 1982, was described by Royer and Emery (1984). Complementary remote sensing and numerical modeling studies are especially important in the case of the Bering Sea due to the remoteness and geographical extent of the region, and the consequent logistical difficulty in field programs.

We have chosen to use the Navy Layered-Ocean Model (Hurlburt and Thompson 1980; Thompson and Schmitz 1989; Wallcraft 1991; Hurlburt et al. 1992), developed over several years at the Naval Research Laboratory–Stennis. The model employs the nonlinear primitive equations in a layered, free surface context that can accommodate realistic basin shapes and bottom topography. The three-layer, hydrodynamic version used here on a 1/8° spherical grid, is well-suited to investigate the seasonal and interannual variability of upper-ocean circulation (the oceanic troposphere, Defant 1936) in a region of meanders and eddylike features such as the Bering Sea. In the next section a brief review of the model formulation is provided. In subsequent sections the mean circulation and variability of the model are described, followed by a discussion of regional features. Intercomparison between the model and observations, particularly those reported in the companion paper (Stabeno and Reed 1994), are made throughout the paper and in the conclusions.

2. Model formulation

The vertically integrated equations of motion, used in the n-layer finite depth hydrodynamic model, are as follows for layers $k = 1, \cdots, n$:

$$\frac{\partial \mathbf{V}_k}{\partial t} + (\nabla \cdot \mathbf{V}_k + \mathbf{V}_k \cdot \nabla)\mathbf{v}_k + \mathbf{k} \times f\mathbf{V}_k$$

$$= -h_k \sum_{l=1}^{n} G_{kl}\nabla(h_l - H_l) + \max(0, \omega_k)\mathbf{v}_{k+1}$$

$$- [\max(0, -\omega_k) + \max(0, \omega_{k-1})]\mathbf{v}_k$$

$$+ \max(0, -\omega_{k-1})\mathbf{v}_{k-1}$$

$$+ (\vec{\tau}_{k-1} - \vec{\tau}_k)/\rho_0 + A_H h_k \nabla^2 \mathbf{v}_k, \quad (2.1)$$

$$\frac{\partial h_k}{\partial t} + \nabla \cdot \mathbf{V}_k = \omega_k - \omega_{k-1}. \quad (2.2)$$

Definitions of the variables and parameters are provided in Table 1; parameter values used for the model runs are listed in Table 2. The model equations are solved numerically on a staggered C grid with zonal and meridional intervals of 13.9 km and 11.5 km at 54°N; a semiimplicit time-differencing scheme is used for all gravity wave components. A no-slip condition is applied at the walls; the boundary conditions at the inflow and outflow ports are discussed below. Additional details of the implementation of the model are given in the user's guide (Wallcraft 1991).

TABLE 2. Parameter values.

$n = 3$	$\sigma_T = 26.34, 26.97, 27.68$
$A_H = 100\ \text{m}^2\ \text{s}^{-1}$	$H_k = 200\ \text{m}, 300\ \text{m}, D - 500\ \text{m}$
$C_b = 0.002$	$h_k^+ = 75\ \text{m}$
$C_k = 0.0$	$h_k^- = 9999\ \text{m}$
$g = 9.8\ \text{m}\ \text{s}^{-2}$	$\tilde{\omega} = 0.01\ \text{m}\ \text{s}^{-1}$

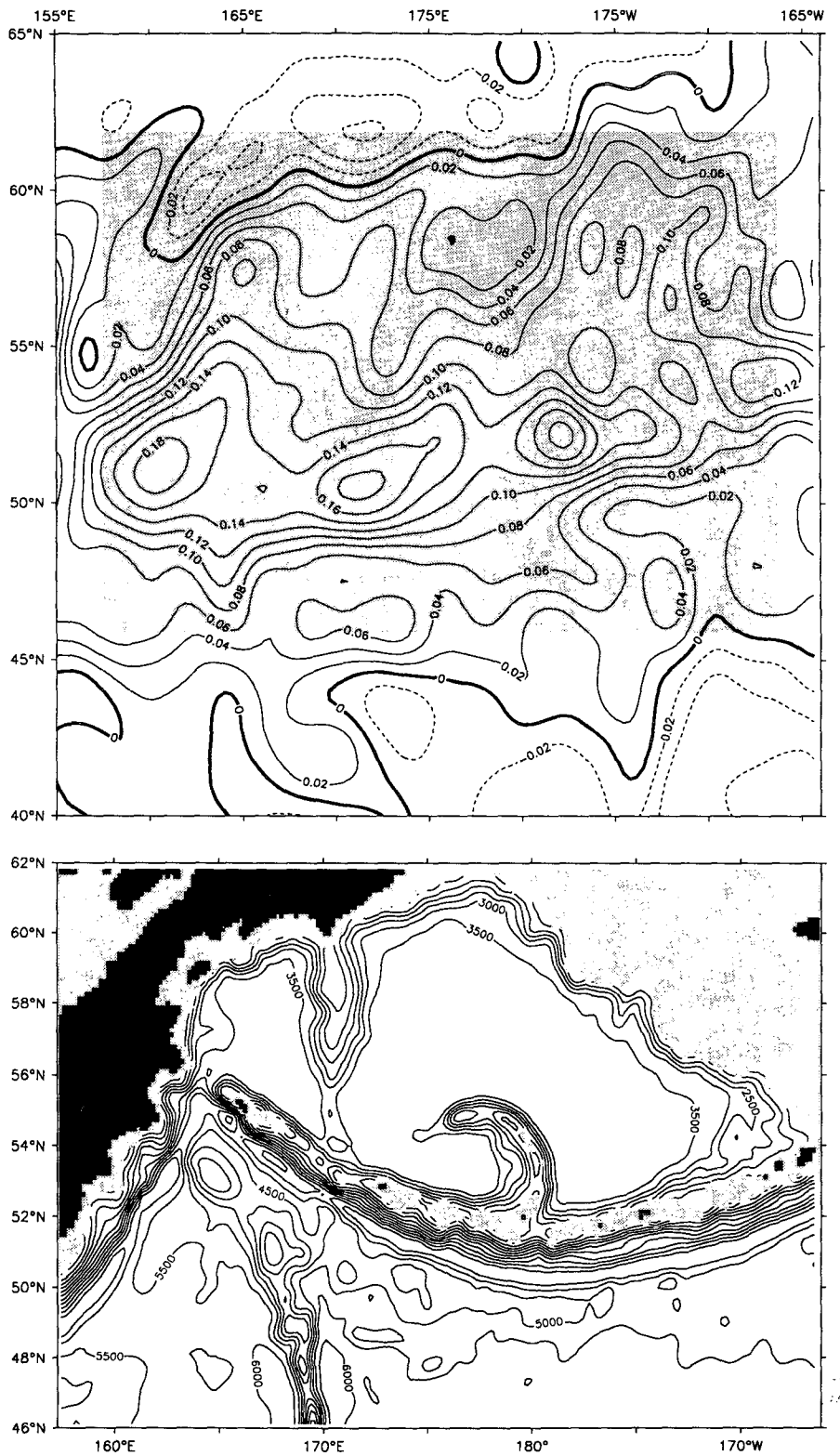

FIG. 2. Upper panel: distribution of annual average wind stress curl in units of newtons per square meter (1000 km)$^{-1}$ based on the Hellerman and Rosenstein (1983) climatology. Lower panel: bathymetry within the model domain (contour interval 500 m); the model excludes shelf regions with depths less than 500 m.

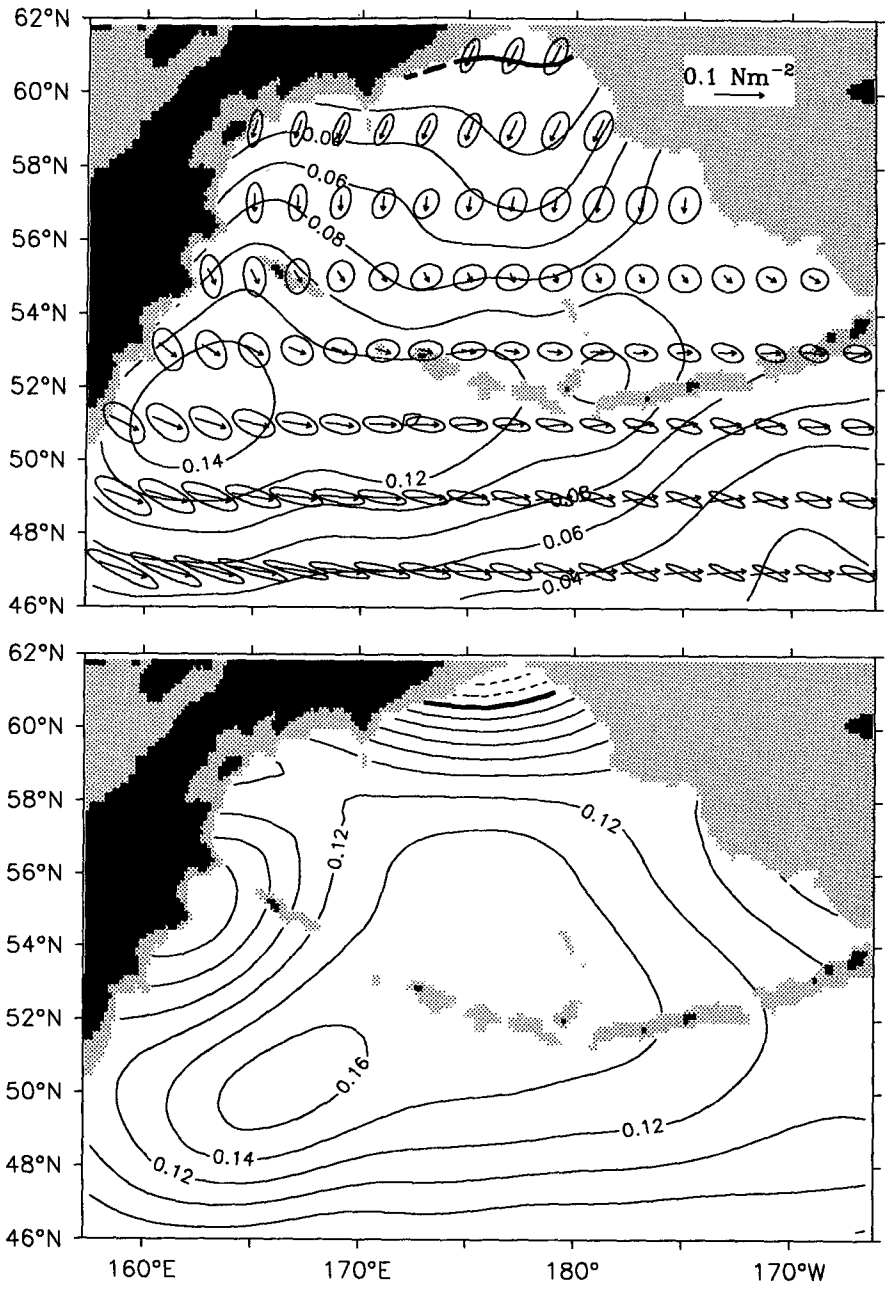

FIG. 3. Upper panel: Annual mean vectors, principal axes ellipses, and curl of the wind stress field employed in the model. Lower panel: Annual average wind stress curl derived from twice-daily NMC pressure fields over the period 1949–1989 (Bond et al. 1994).

Much of the vertical density structure of the Bering Sea can be represented by a surface layer, about 200 m thick, and a deeper transition near 500 m (Takenouti and Ohtani 1974). A three-layer model formulation with mean upper and middle layer thicknesses of 200 m and 300 m, respectively, is chosen; the modal structure was not explicitly calculated. The density in each layer is set to the annual mean over the model domain of the Levitus (1982) climatology. A constraint of the model formalism is that layer interfaces must intersect a vertical wall, that is, that bathymetry be entirely in the deepest layer. As a result, Bering Sea shelf and slope regions shallower than 500 m are explicitly excluded from the model. Because a goal of the study is to develop an understanding of the transport through the Aleutian passes, the bathymetry of Amukta Pass, whose sill depth is somewhat less than 500 m, has been artificially increased. The model provides for an enhanced

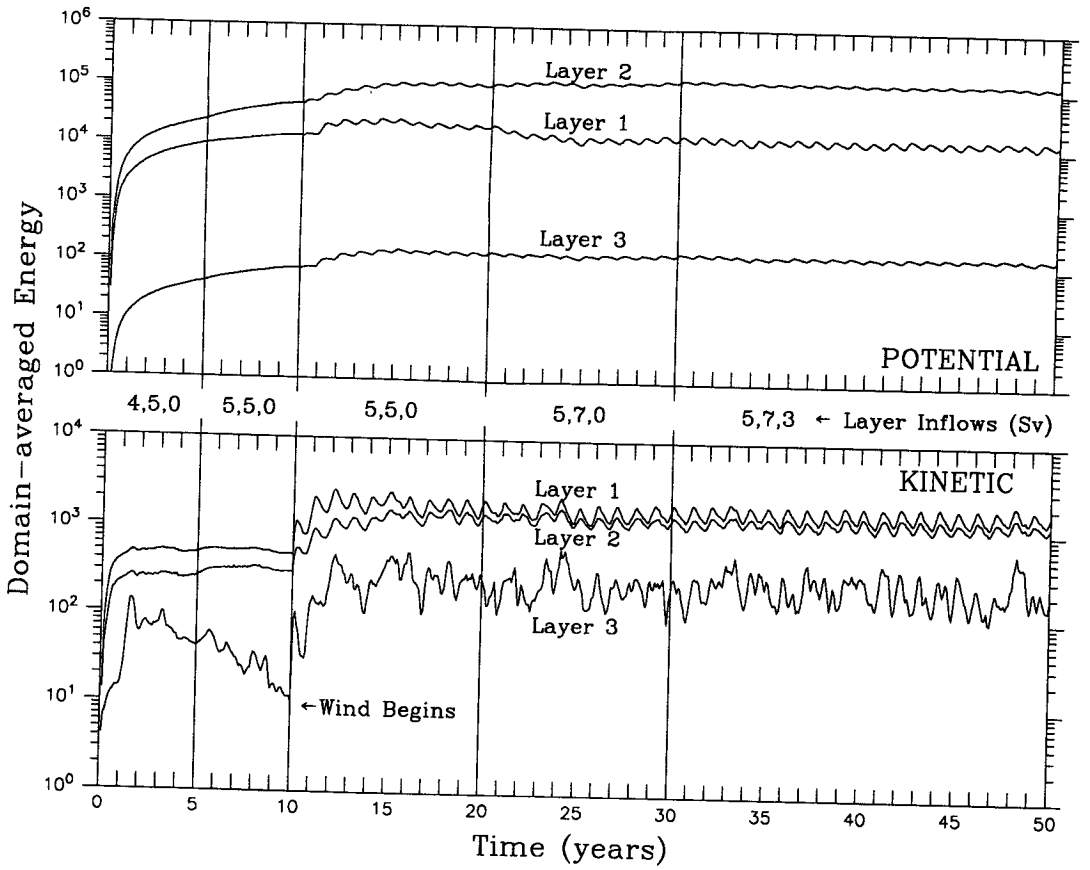

FIG. 4. Spinup of the model over a 50-year period as illustrated by the domain-averaged potential and kinetic energies in each layer. The wind is turned on after the first 10 years; the inflow is increased in steps as indicated between the panels to a final state with 5, 7, and 3 Sv of inflow in the upper, middle, and lower layers, respectively.

friction coefficient in such regions to attenuate the spurious lower-layer transport.

The model domain is chosen to reflect our interest in regional circulation patterns induced by wind forcing and the Alaskan Stream. The southern boundary is a vertical wall at 46°N, which is close to the zero crossing of the climatological wind stress curl. As seen in Fig. 2a, the mean annual wind stress curl, based on the Hellerman and Rosenstein (1983) winds, is positive over the model domain. The eastern and western bounds of the domain are near 166°W and 157°E. The former is represented by a vertical wall, except where the Alaskan Stream inflow is prescribed, while the boundary south of Kamchatka is open to permit outflow. Figure 2b shows the total water depth at rest employed for the model. This is based on the ETOPO5 database of world bathymetry, discretized to the model grid and weakly smoothed with a nine-point filter (Shapiro 1970).

The circulation of the model Bering Sea and north Pacific Ocean is driven by the throughput of the Alaskan Stream and by the winds. The Alaskan Stream enters at the eastern boundary, just south of the Alaskan peninsula. Observations (Reed 1984; Stabeno and Reed 1991) and modeling (Cummins 1989) show that this boundary current has little or no seasonal cycle, and very little eddy energy at the longitude at which it enters the model domain. As a result the stream is modeled as a constant inflow, directed alongshore and uniformly distributed across a 1° inflow port centered at 52°45'N. When fully spun up in the model runs described here, the Alaskan Stream has 15 Sv of transport with 5, 7, and 3 Sv in the upper, middle, and lower layers, respectively. The outflow port lies between the tip of the Kamchatka Peninsula and the southern wall of the model domain at 46°N. The outflow boundary condition (Wallcraft 1991) is a modified Orlanski (1976) radiation condition, with a linear implicit drag at points for which inflow is predicted. This serves to prevent the development of unrealistic recirculation loops at the opening while permitting, by a suitable choice of drag coefficient, waves and eddies to migrate out of the region. For each time step the net outflow in each layer is required to match the corresponding inflow from the Alaskan Stream; there is no provision for temporary storage of excess mass within the overall model domain.

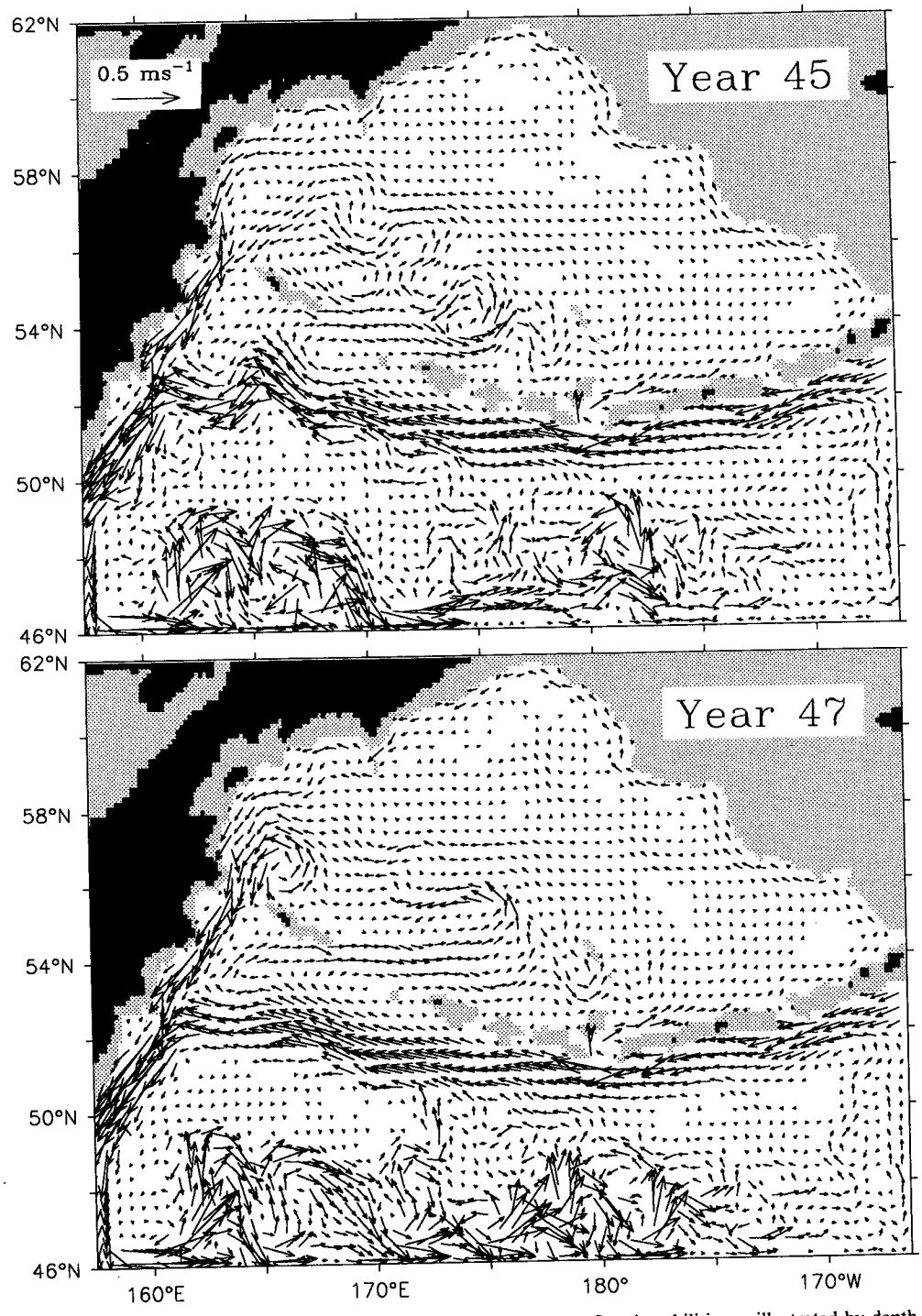

FIG. 5. Interannual differences in upper-layer circulation due to flow instabilities as illustrated by depth-averaged currents on the first day of January in successive model years. For years 45 and 47 the entire domain

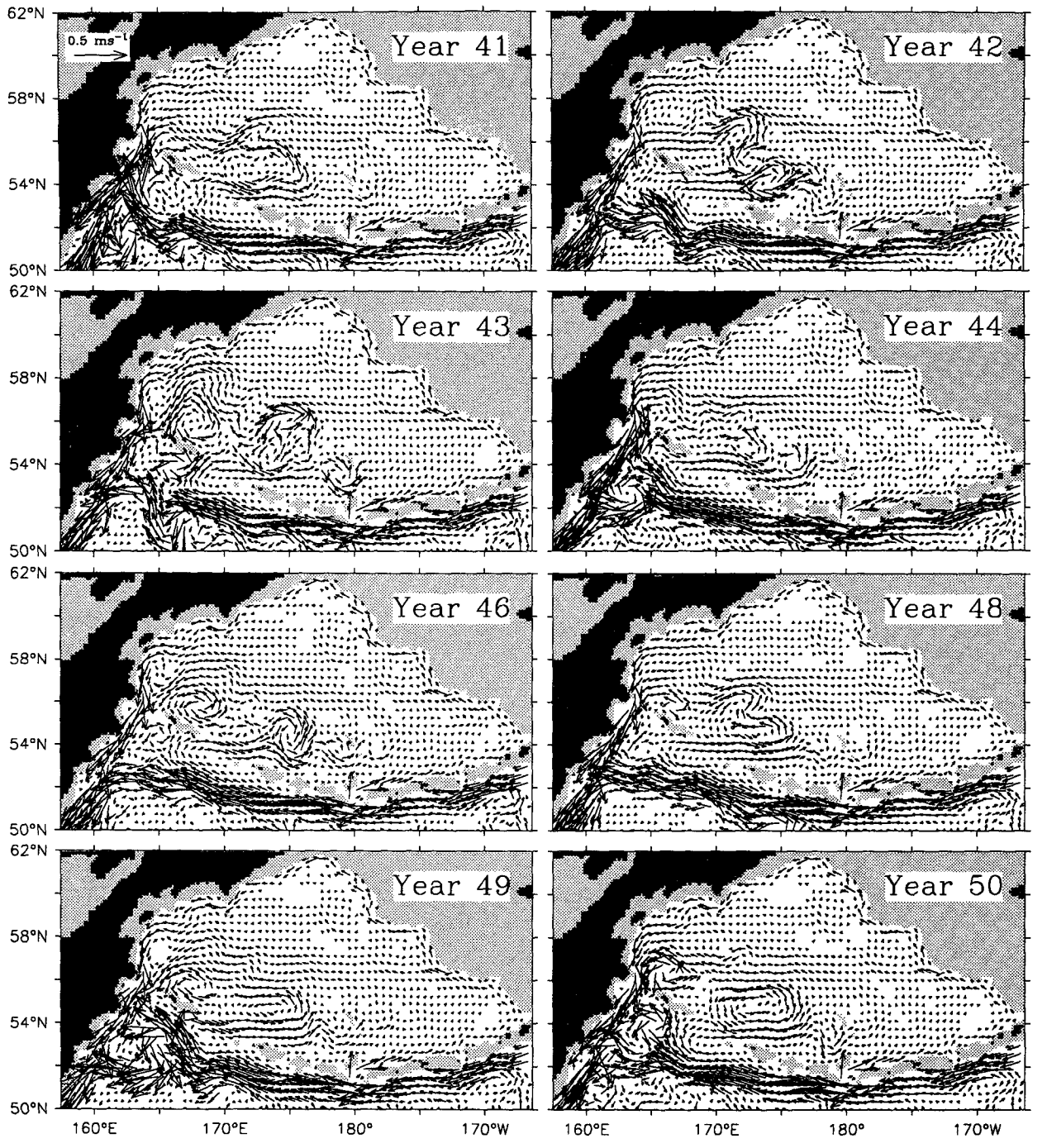

FIG. 5. (*Continued*) is shown, for other years only the region of primary interest north of 50°N. The model was forced by the Hellerman and Rosenstein (1983) monthly wind stress climatology.

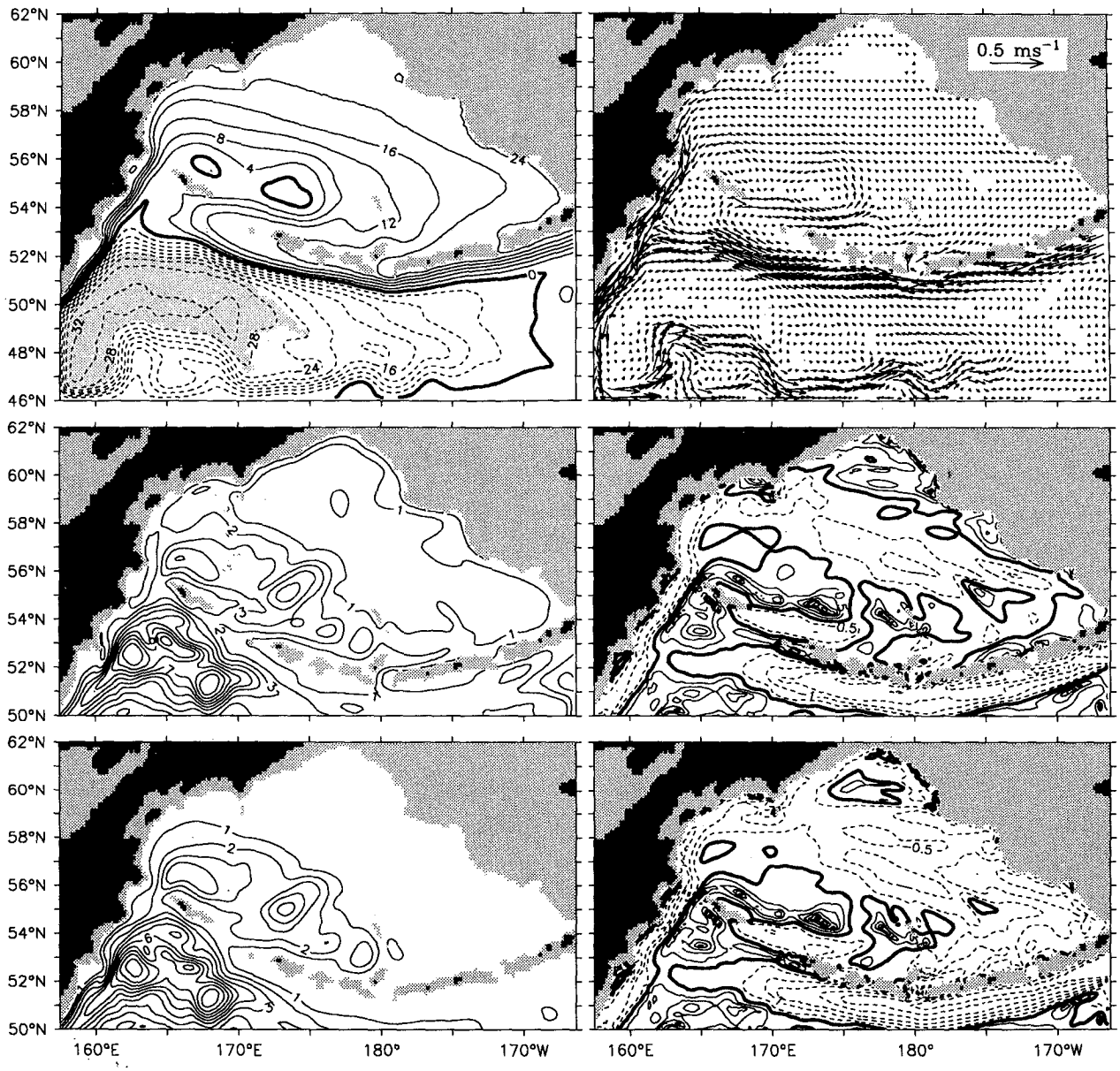

FIG. 6. Summary statistics for sea level (left column) and upper-layer circulation (right column) in the final decade of the model run. Top row: mean sea level (cm) and depth-averaged upper-layer current vectors. Middle row: overall variability relative to the 10-year mean. Bottom row: anomaly variability in which the seasonal cycle has been removed. For sea level the standard deviation is the measure of variability; for circulation the common logarithm of the kinetic energy ratio $(\sigma_u^2 + \sigma_v^2)/(\bar{u}^2 + \bar{v}^2)$ is used. Here σ_u^2, σ_v^2, $\bar{u}$, and $\bar{v}$ are the variances and means of the zonal and meridional velocity components. Dashed isopleths correspond to relatively steady currents. The shaded region of the western subarctic gyre in the upper-left panel indicates where hydromixing in the model is likely to occur.

Periodic wind forcing is applied to the model based on the Hellerman and Rosenstein (1983) monthly climatology. Wind stresses were interpolated in space to the model grid using cubic splines to provide a smooth wind stress curl. The interpolation in time is linear between the monthly fields, and the annual wind cycle is repeated over each successive 366-day model year. The annual mean of the wind stress and wind stress curl fields are shown in Fig. 3a, together with the principal axis ellipses of the wind stress variability. These agree quite well with wind stress climatological estimates (Fig. 3b) based on the twice daily NMC (National Meteorological Center) pressure fields over the period 1946–1989 (Bond et al. 1994). The Hellerman–Rosenstein curl is weaker than the NMC curl in the central Bering Sea basin.

The terms involving ω are associated with an optional "hydromixing" feature of the model (Wallcraft

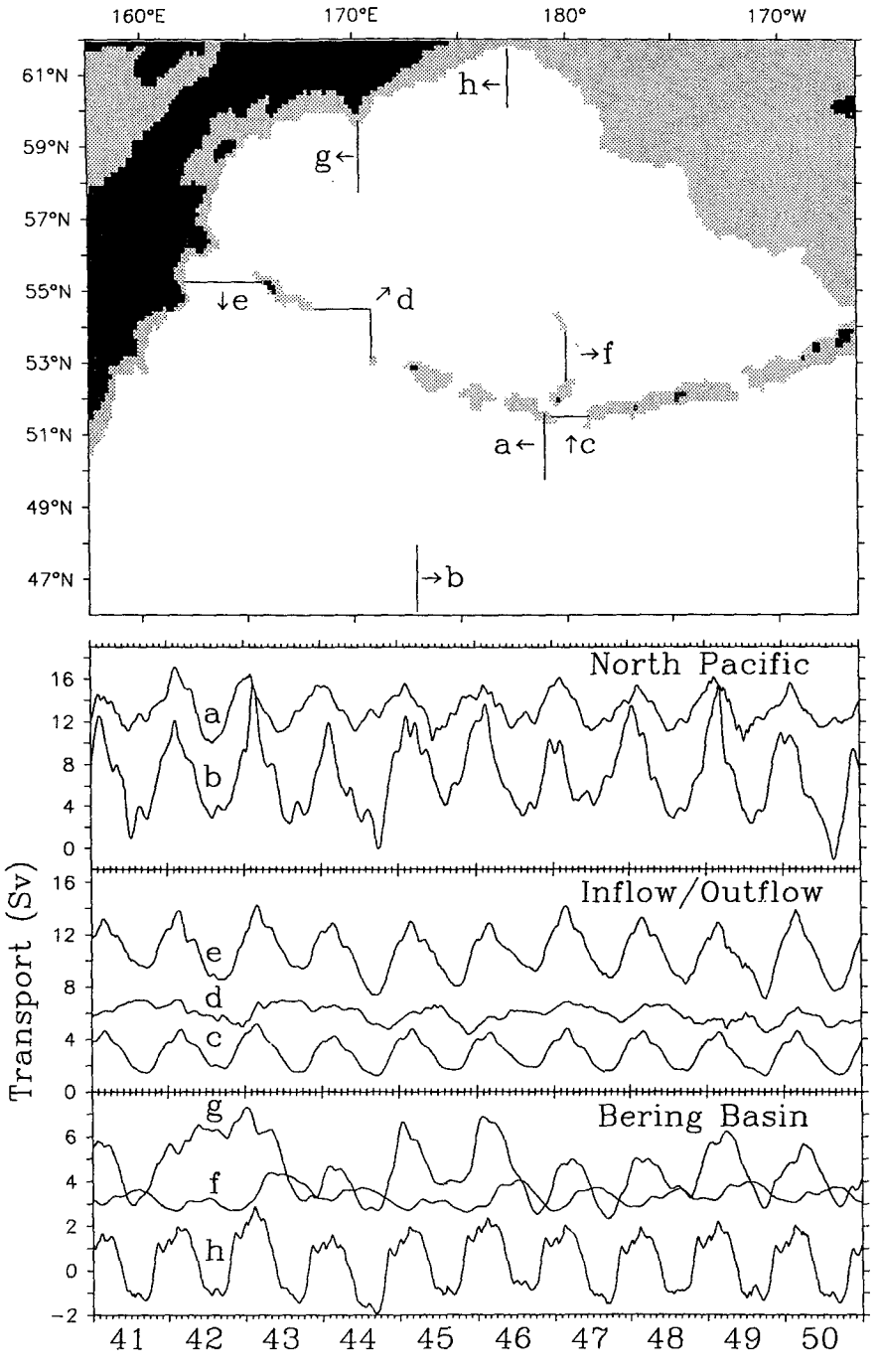

FIG. 7. Time series of selected total transports over the last 10 years of the model run. The sections are (a) Alaskan Stream near the date line, (b) recirculation along the lower boundary of the model domain, (c) inflow through Amchitka Pass, (d) inflow through Near Strait, (e) outflow through Kamchatka Strait, (f) eastward flow over Bowers Ridge, (g) westward flow over Shirshov Ridge, and (h) reversing flow in the northern Bering basin.

TABLE 3. Autocorrelation time scales for sea level and velocity at selected locations within the model domain (see Fig. 8). Subscripts 1, 2, and 3 denote upper-, middle-, and lower-layer velocity fields.

Location	Latitude (°N)	Longitude	Variable	Time scale (days)
A	54.0	175.0°W	Sea level	45.3
			(u_1, v_1)	42.6
			(u_2, v_2)	42.0
			(u_3, v_3)	52.1
B	55.0	163.0°E	Sea level	51.0
			(u_1, v_1)	67.2
			(u_2, v_2)	71.4
			(u_3, v_3)	29.1
C	60.0	180.0°	Sea level	171.6
			(u_1, v_1)	57.2
			(u_2, v_2)	56.1
			(u_3, v_3)	40.3
D	56.0	172.0°W	Sea level	165.6
			(u_1, v_1)	56.1
			(u_2, v_2)	56.8
			(u_3, v_3)	47.4
E	51.8	179.5°W	Sea level	176.6
			(u_1, v_1)	46.6
			(u_2, v_2)	49.7
			(u_3, v_3)	39.2
F	54.0	170.0°E	Sea level	151.1
			(u_1, v_1)	123.2
			(u_2, v_2)	69.0
			(u_3, v_3)	47.8
G	54.8	174.0°E	Sea level	152.3
			(u_1, v_1)	118.1
			(u_2, v_2)	142.0
			(u_3, v_3)	115.7
H	50.5	167.0°E	Sea level	165.3
			(u_1, v_1)	96.3
			(u_2, v_2)	100.3
			(u_3, v_3)	92.4

1991). This serves to inhibit the surfacing of layer interfaces; when the local thickness of a layer becomes less than a preset minimum, water is entrained from adjacent layers to counter the trend. A complementary mechanism of local detrainment can be invoked if the thickness of a layer exceeds a preset maximum. When hydromixing occurs there is a regionwide detrainment or entrainment to maintain the constancy of layer volumes.

The upper and middle layers tend to surface in the western subarctic gyre region of the model domain. The tendency is countered by invoking hydromixing when layer thicknesses fall below 75 m; no preset maximum is required. At 50.5°N, 167°E conditions favoring hydromixing prevail in the final decade of the model run; substantial deepening of the upper layer is confined to model year 42 when, as described in a later section, a major meander formed in the Alaskan Stream to the south of Near Strait.

The model time step of 48 minutes permits long integrations and the model is spun up from rest over a 40-year period. A further 10 years are simulated to provide circulation statistics. For the first decade no wind forcing is applied; the Alaskan Stream is built up in steps to its final state over the first 30 years. The spinup of the domain-averaged potential and kinetic energies is shown in Fig. 4. A quasi-periodic annual cycle is established; some interannual variability is present, most noticeably in the lower layer. The spinup history depicted in Fig. 4 is quite robust. Earlier runs with model geometries including lesser areas of the North Pacific and differing outflow port locations produced similar spinup histories and area-averaged energy levels.

3. Model statistics

The state of the model, interface displacements, and transports in each layer was archived at 6-day intervals during the final decade of the 50-year run. Although the forcing by the Alaskan Stream is constant and the wind forcing periodic, the model response exhibits strong interannual variability associated with the generation of mesoscale features within the domain. Figure 5 shows depth-averaged currents in the upper layer for the first day of January in model years 41–50. For years 45 and 47 the entire domain is shown, while for the other years of the decade the panels are truncated at 50°N. To the west-northwest of Bowers Ridge strong interannual differences in eddy activity are evident. In January of year 45 the region contains a train of eddy features; in year 47 the circulation in this region is far less complex. Along the eastern side of the basin eddies form and propagate in a well-defined annual cycle. The Alaskan Stream becomes unsteady west of 170°E, with occasional meandering and eddy shedding episodes that influence the major inflow to the Bering Sea via Near Strait. There are strong meanders along the southern arm of the western subarctic gyre, particularly upstream of the topographic ridge near 170°E. Recirculation into the Alaskan Stream is distributed across the width of the model domain and it appears that the aphysical presence of a wall at 46°N is not adversely influencing the region of primary interest north of 50°N.

Summary statistics for the mean (top panels) and variability of sea level and upper-layer currents over the decade are shown in Fig. 6. Sea level variability is expressed as the standard deviation, while variability in upper-layer circulation is shown as a kinetic energy ratio,

$$(\sigma_u^2 + \sigma_v^2)/(\bar{u}^2 + \bar{v}^2),$$

contoured on a common logarithmic scale. Here σ_u^2, σ_v^2, $\bar{u}$, and $\bar{v}$ are the variances and means of the zonal and meridional velocity components. Both the overall and the anomaly variability are drawn since in some regions, notably the eastern side of the basin, the sea-

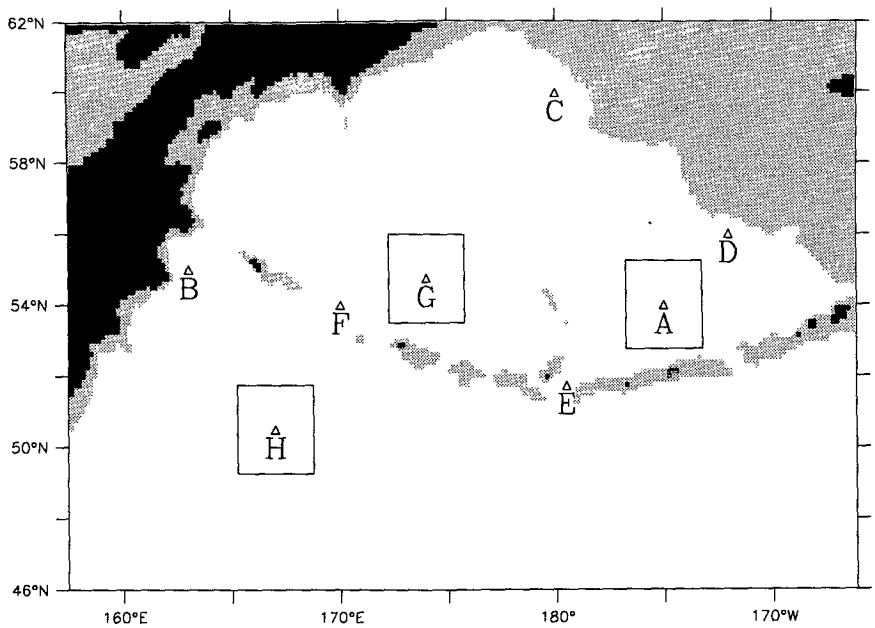

FIG. 8. Locations (denoted by triangles) for which the autocorrelation time scales of Table 3 were computed. Rectangles indicate subregions for which the spatial correlation patterns of Fig. 9 are drawn.

sonal cycle is dominant. The overall variability is computed relative to the 10-year mean; anomaly variability is computed having first subtracted the appropriate monthly means, over the 10-year period, from each image.

The model Alaskan Stream region (defined to be steady at inflow) is stable with variability of a few percent east of 170°E. To the west it bifurcates with a portion separating from the Aleutian arc to join the Kamchatka Current as part of the western subarctic gyre. The remainder turns northward and eastward to enter the Bering Sea via Near Strait. The zonal nature of the inflow to the Bering Sea at Near Strait is in strong contrast to the northeastward flow indicated in the earlier circulation schematics (e.g., Hughes et al. 1974). The model result is consonant with the satellite-tracked buoy results of Royer and Emery (1984) and Stabeno and Reed (1994). In the region south of the Komandorski Islands (165°–170°E), strong meanders may develop in the Alaskan Stream, as shown theoretically by Thomson (1972), and in the model of Cummins and Freeland (1993). The model Kamchatka Current is a region of low variability and lacks the meanders occasionally seen in satellite-tracked buoys within the Bering (Stabeno and Reed 1994).

There is a generally eastward flow along the northern flank of the Aleutian Islands. A substantial portion is deflected northward at Bowers Ridge both in the model and in satellite-tracked buoy observations (Stabeno and Reed 1994). The eastward flow is augmented near 180° by an inflow through Amchitka Pass. The inflow through the other passes has been forced to be minor by choice of the local friction in accord with prior knowledge of their influence (Schumacher et al. 1982; Reed 1990). The return flow westward across the basin is broad and quite steady, feeding into the Kamchatka Current. The flow near the shelf in the eastern and northern Bering Sea is variable. Eddylike features develop near 58° and 60°N in late summer and fall, which cause a reversal of the flow along the shelf. Observed buoy tracks (Stabeno and Reed 1994) tend to separate from the eastern shelf near 57°N in accord with these eddy features in the model.

In Fig. 6, there is a region of high eddy activity to the west of Bowers Ridge near 55°N. The main eddy near 174°E is a cyclonic quasi-permanent feature throughout the simulation, varying in strength and position although never reversing; it occasionally joins the more intermittent feature near 178°E. North of the Komandorski Islands is another intermittent counterclockwise eddy feature that results in an eastward shelf flow that is strongest in the summer and fall. On occasion there can be inflow to the Bering Sea through the eastern portion of Kamchatka Strait. These events are associated with large meanders that form in the Alaskan Stream west of 170°E.

The southern portion of the model domain represents the North Pacific and is of little interest, per se, to this study. Its meridional width is intended to isolate the region of interest from the artificial walls at the southern and eastern boundaries. This goal appears to be realized to the extent that there is a general eastward

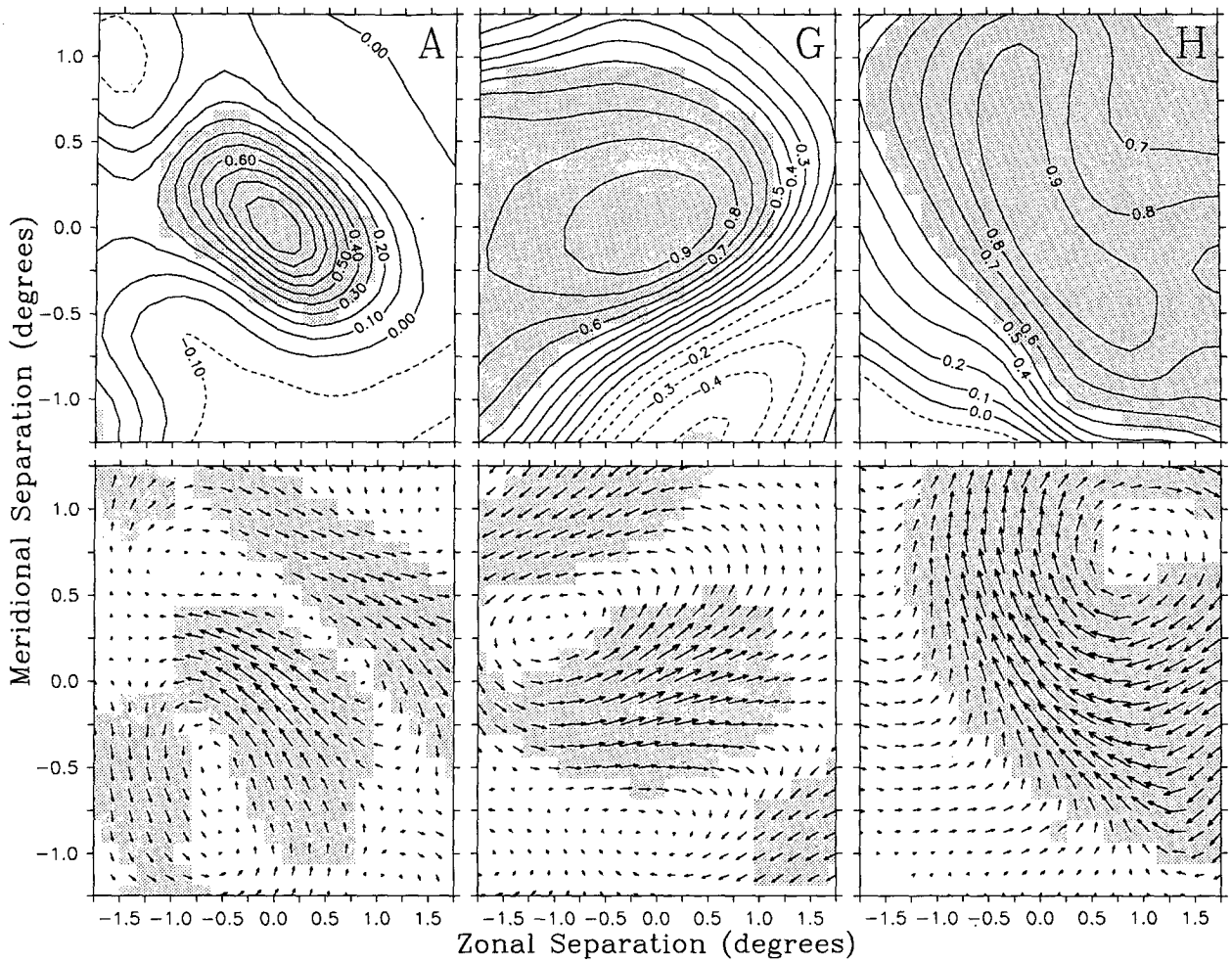

FIG. 9. Patterns of spatial correlation in sea level (top row) and upper-layer velocity (bottom row) anomalies for the subregions A, G, and H of Fig. 8. The correlations (highlighted when significant at the 99% significance level) are shown for space lags up to ±10 model grid cells from the central point; axis units are in degrees east–west and north–south. Correlations in the velocity field are represented by a vector field based on the magnitude and argument of the complex correlation coefficient. The vector at the central point has unit magnitude and is oriented along the principal axis of local variability, while other vectors indicate the current direction best correlated with the central time series. Space scales are shorter in the eastern Bering Sea (A) than in the regions west of Bowers Ridge (G) or south of the Komandorski Islands (H); asymmetry in the correlations are associated with recurring eddy or meander patterns in the circulation.

flow in the south mimicking the western subarctic gyre, some recirculation into the Alaskan Stream throughout its length, and no major northward flow along the eastern boundary. Shaded in the upper-left panel of Fig. 6 is the region where mean upper-layer thickness lies within one standard deviation of 75 m. Hydromixing is likely to be frequent in this portion of the western subarctic gyre, but is not a factor within the areas of our prime concern. The portion of the model domain south of 50°N is excluded from most of the following discussion and graphics.

In Fig. 7 the time series of transport, summed over the three layers, are plotted for selected sections. These section transports were sampled daily for the final decade of the model run. There is a pronounced seasonal cycle at most sections. A large amplitude variation in the eastward flow along the southern boundary (section b) imposes a seasonal variation of about 6 Sv in the Alaskan Stream near 180° (section a). Recall that the prescribed inflow of the stream is 15 Sv. The inflow to the Bering Sea through Near Strait (section d) exhibits a greater interannual variability than does that through Amchitka Pass (section c), or the combined outflow through Kamchatka Strait (section e). While the model inflow through Amchitka Pass does not reverse, as reported by Reed (1990), it is at its weakest at the appropriate time (August–October). Within the Bering Sea there is a consistent eastward flow over Bowers Ridge (section f). The interannual variability in this flow is only partly explained by the fluctuations in the Near Strait inflow. At the north of the basin (section h), the transport reverses from westward, between late

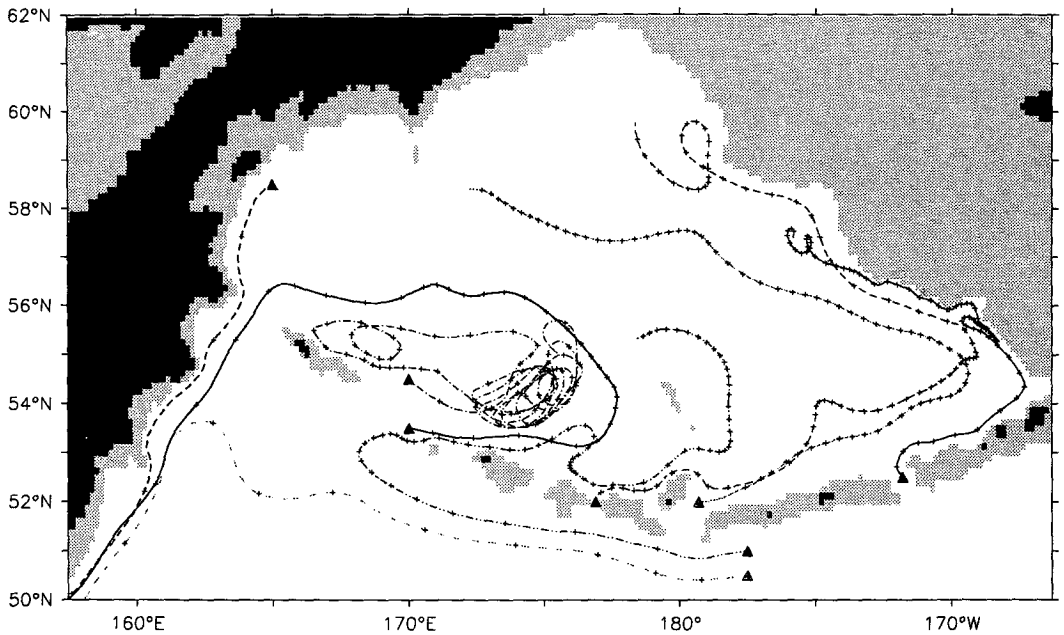

FIG. 10. Samples of 2-year simulated buoy tracks illustrating major features of the circulation of the Bering Sea basin and the adjacent North Pacific Ocean. Triangles are the starting points and tick marks are 10-day intervals.

fall and spring, to eastward in the summer and early fall. The source region of the Kamchatka Current near Shirshov Ridge (section g) exhibits considerable interannual variability. In the satellite-tracked buoy results of Stabeno and Reed (1994), the northern portion of the Bering Sea basin exhibits considerable eddy activity but the temporal sampling is inadequate to confirm or refute the organized seasonal reversals suggested by the model.

The correlation functions of the time series from discrete locations have been examined to gain insight into the temporal and spatial scales of the model response. If the time scale is defined as the integral of the autocorrelation function to its first zero crossing, then the model response in general reflects the long time scales inherent in the monthly climatological wind forcing of typically 1–2 months. Table 3 lists time scales for selected model variables at the locations depicted in Fig. 8. The slow evolution indicated suggests that monthly images of model output will suffice to describe most features. The spatial structures of correlation in sea level and upper-layer velocity anomalies are shown in Fig. 9 for three regions. For sea level the contours represent the correlation (at zero time lag) between the central point and the model grid points that surround it. For the velocity field the complex correlation (Kundu 1976) is used, which gives the rotation angle of the component best correlated with the vector series at the central point. In Fig. 9 the complex correlations are represented as vectors whose lengths are proportional to the correlation. The central vector has unit magnitude and is oriented along the major axis of local variability. Correlations exceeding the 99% confidence level, based on the degrees of freedom at the central point, are highlighted. In the eastern Bering Sea basin (A) the spatial scale of the sea level field is short, but the upper-layer velocity field has a banded structure about a southeast–northwest axis associated with a meandering of the current near 54°N, 175°W (see Fig. 15). In the region west of Bowers Ridge (G), the spatial scale of sea level anomalies is large, extending westward beyond the selected subregion. Both sea level and upper-layer velocity correlation are banded along a northwest–southeast axis, consistent with the wave trains that occasionally propagate northwestward through this region (Figs. 5 and 14). South of the Komandorski Islands the correlation patterns for both sea level and velocity reflect the structure of the Alaskan Stream. Spatial scales are large along the axis of the stream and the rotation angles suggest the southward meanders of the stream axis in this region (see Fig. 13).

4. Simulated buoy tracks

Because much of our knowledge of upper-layer circulation in the Bering and Alaskan Stream regions is being acquired through the use of satellite-tracked buoys drogued at 40 m or 100 m (Stabeno and Reed 1994), it is instructive to simulate such tracks in the model. At every second time step the velocity field is linearly interpolated to the previous buoy position. Using the Adams Extrapolation Formula (Abramowitz and Stegun 1964), the position is then updated using the latest and three previous velocity interpolations.

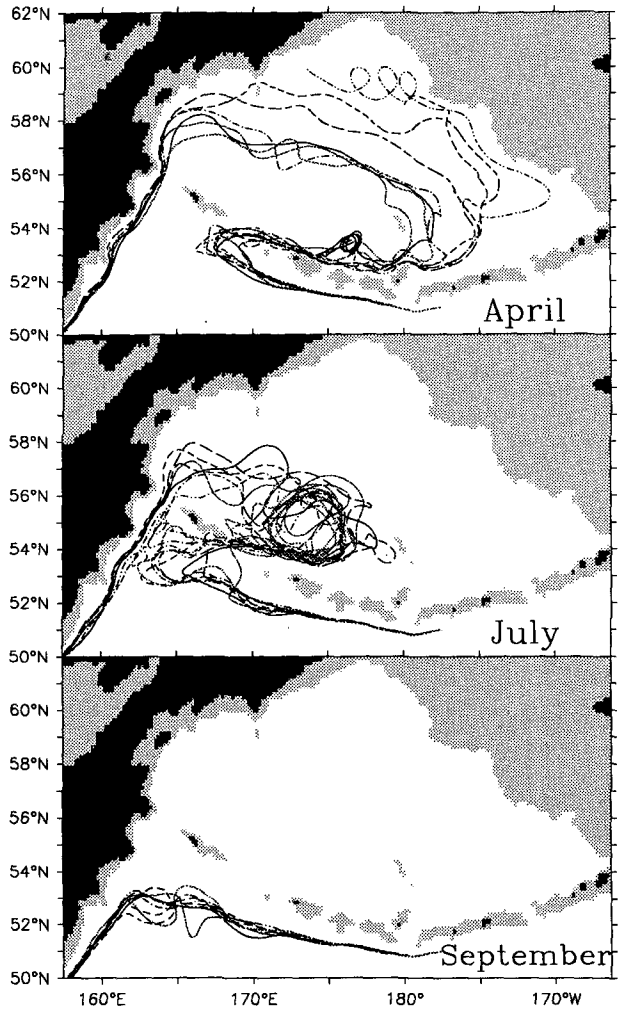

FIG. 11. Seasonal differences in the trajectories of simulated buoys deployed at a common starting point on the northern flank of the Alaskan Stream. Each panel shows eight releases (model years 41–48) beginning on the first day of the indicated month. Buoys released in April enter the Bering Sea via the eastern side of Near Strait and traverse the eastern portion of the basin. Those released in July enter via the western side of Near Strait and do not reach the eastern basin. Buoys released in September avoid the Bering Sea basin.

In Fig. 10, 2-year buoy tracks are presented, with tick marks indicating positions at 10-day intervals. All were released on the first day in January in model year 41 at the locations marked with triangles. Buoys released in the passes east of 170°E track eastward along the northern flank of the Aleutian chain before moving northwestward. The simulated buoy released in Amukta Pass (172°W) hugs the slope of the Bering Sea shelf. Actual buoys traversing this region tend to make excursions onto the shelf, which is excluded from the model domain. The simulated buoys are sluggish compared to their real counterparts, which typically exit the Bering Sea, via Kamchatka Strait, in 15–18 months. This is to be expected because the mean model upper-layer depth in the eastern Bering is about 250 m, considerably larger than the drogue depth of the actual buoys.

A model buoy released in the path of the inflow through Near Strait exits the basin via Kamchatka Strait in about 9 months, while another, released 1° north of the inflow, gets trapped in the eddy region west of Bowers Ridge. The strength of the outflow through Kamchatka Strait is evident. Buoys on the landward side of the Kamchatka Current exit the model domain through the outflow port; others may move south to join the eastward current along the wall at 46°N. A similar divergence is evident in the behavior of model buoys released on the northern and southern flanks of the Alaskan Stream near 179°W. Buoys released on the northern flank enter the Bering Sea mainly via Near Strait. Buoys released on the southern flank generally avoid the Bering and either exit the outflow port or rejoin the Alaskan Stream via the western subarctic gyre.

The behavior of model buoys released near 52°N, 178°W has been investigated in greater detail. Buoys were released at monthly intervals (the beginning of each model month of 30.5 days) during years 41–48 of the model run, providing eight realizations for each release date. Between the release point and 173°E the drift paths are almost coincident; beyond this point divergence occurs and a seasonal pattern in drifter paths emerges. Figure 11 illustrates the discussion for April, July, and September.

For release dates early in the year the simulated buoy tracks recurve at about 169°E and all enter the Bering through the eastern side of Near Strait. For later release dates the point of recurvature moves westward until, for June and July release dates, some buoys join the Kamchatka Current between 52° and 54°N and move south. The remainder travel as far west as 163°W before turning northward and eastward, entering the Bering through the western side of Near Strait. For August the trend continues with only three of the eight simulated buoys entering the Bering through Near Strait. Another buoy makes a short incursion to the Bering Sea through the eastern side of Kamchatka Strait. Buoys released in September and October, without exception, avoid the Bering entirely. Return to the inflow pattern begins with the November releases of which two enter the Bering via Near Strait, three enter via the eastern side of Kamchatka Strait (one of these travels eastward almost to Bowers Ridge), while three avoid the Bering entirely. All eight of the successive December releases enter the Bering via Near Strait. The buoys that do not enter the Bering traverse the region south of the Komandorski Islands between mid-October and early January. Several satellite-tracked buoys, released near Kodiak Island (57°N, 155°W) as part of the FOCI study of Shelikof Strait, were carried westward by the Alaskan Stream. Unfortunately all but one went aground on the Aleutian Islands or entered the Bering

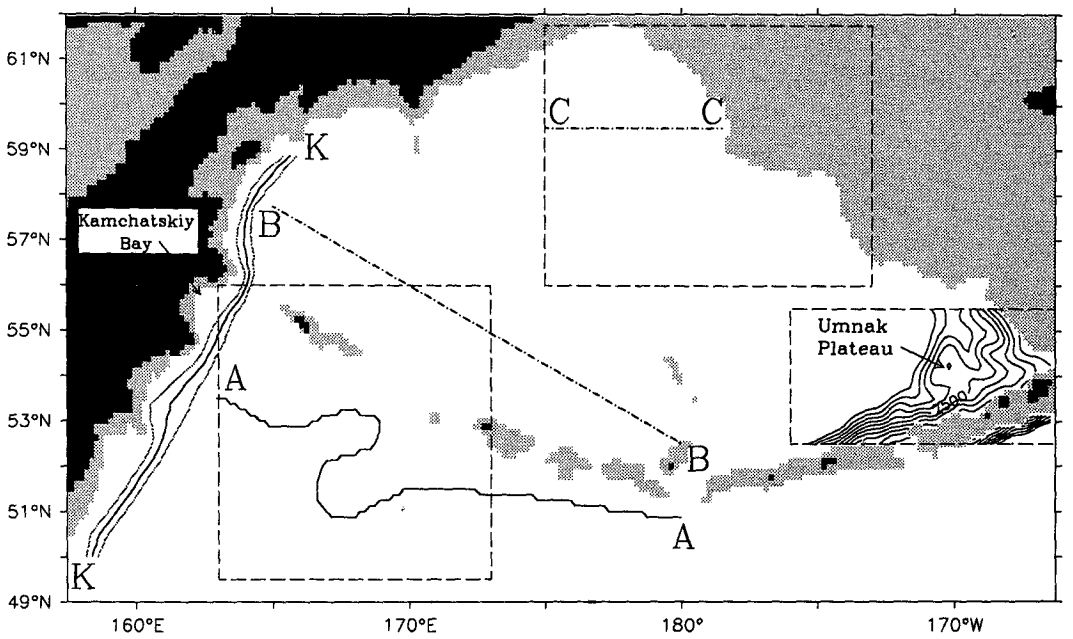

FIG. 12. Locator chart for the discussion of regional features of the circulation. The curve AA is a snapshot of the axis of the Alaskan Stream prior to an eddy-shedding event; KK is the mean axis of the Kamchatka Current; BB and CC are sections for space–time representations.

via the eastern passes. This single buoy followed a path quite like those in the lower panel of Fig. 11. Its passage south of Near Strait in December conforms with model prediction.

There is also a seasonal pattern to the portion of the simulated drift tracks that lie within the Bering. For release dates between December and June the bulk of the tracks extend east of Bowers Ridge (180°). Releases in July, August, and November that enter the Bering Sea remain in the area of eddy activity north and east of Near Strait and do not traverse the eastern portion of the basin.

5. Regional features of the circulation

Figure 12 illustrates a number of subregions of the model domain for which the circulation is described in more detail.

a. The Alaskan Stream

The simulated buoy tracks of the previous section, and the earlier description of flow variability (Fig. 6), illustrate the stability of the model Alaskan Stream east of 170°E. Beyond this point large amplitude meanders may occur. The curve AA in Fig. 12 shows the axis of the stream, in July of model year 42, through a region south of Near Strait and the Komandorski Islands for which monthly upper-layer circulation patterns are presented in Fig. 13. In March and April a southward meander develops, which seems likely to pinch off. This does not occur but a northward loop of the stream continues to intensify until in July it pinches off. The eddy persists for several months into the next year before being entrained in the Kamchatka Current. One other eddy-shedding event occurs in the decade; in model year 48 another large meander develops that, over a period of 30 months, pinches off one eddy to the south and two to the north. The diameter of the eddies is approximately 100 km.

b. Bowers basin

The region to the west and north of Bowers Ridge exhibits persistent eddy activity, as evident in the 2-year trapping of a simulated buoy in Fig. 10 and in satellite-tracked buoy observations (Royer and Emery 1984; Stabeno and Reed 1994). Occasionally, as in the panel for year 45 in Fig. 5, the eddies form trains with a southeast to northwest alignment. Eddy trains in this general region were reported by Solomon and Ahlnäs (1978) in infrared satellite imagery. Figure 14 shows the space–time evolution of sea level along the diagonal section BB of Fig. 12. The center of eddy activity near 174°E is a region of low sea level, while to the west the contour lines suggest propagation along the section at about 0.3 km day^{-1}.

c. Southeast Bering basin

The bathymetry of this region is complex (see Fig. 12), including the Umnak Plateau extending to the

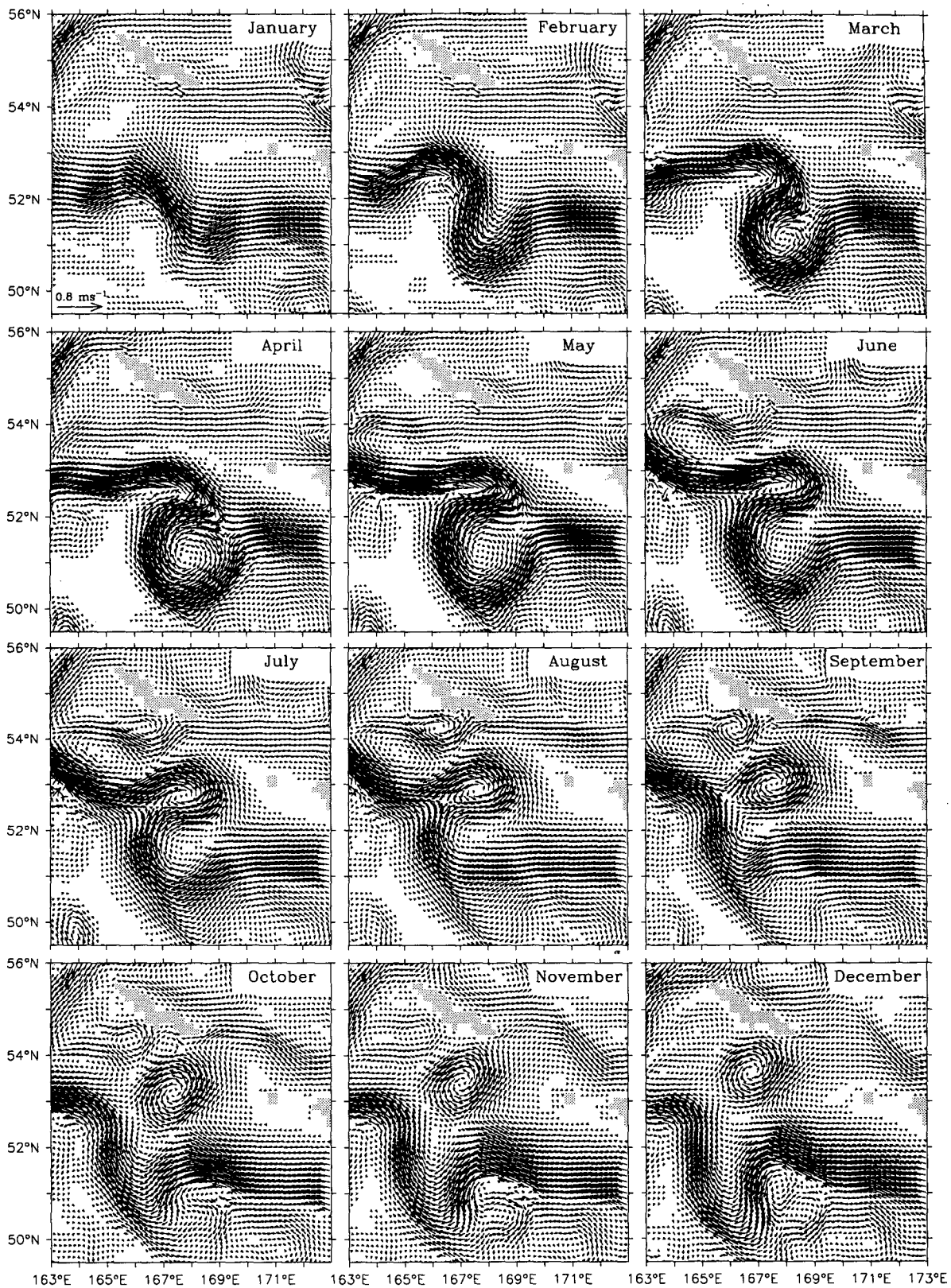

FIG. 13. The development of a meander in the Alaskan Stream during model year 42. The upper-layer circulation, in the subregion delineated in Fig. 12, is drawn at monthly intervals and illustrates one of two major eddy-shedding episodes in the final decade of the model run.

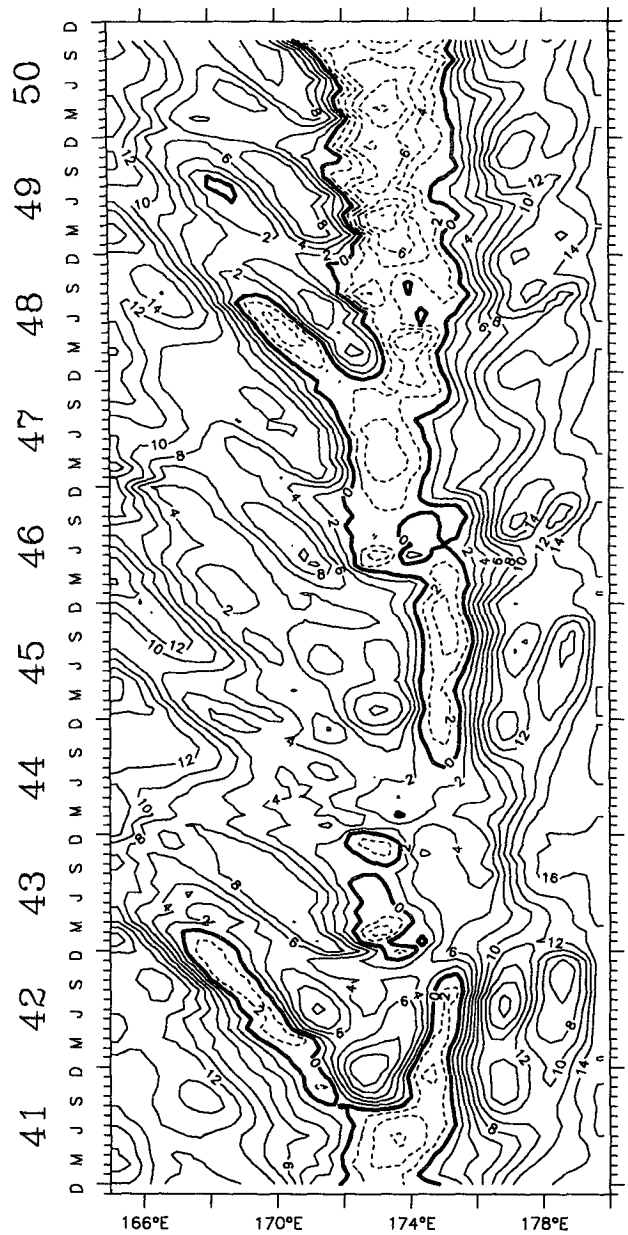

FIG. 14. Space–time evolution of sea level along a diagonal section through Bowers Basin (BB in Fig. 12). The center of eddy activity at 174°E has persistently low sea level, while to the west the contours suggest propagation of eddy trains.

Northwest from Bogoslav Island (54°N, 168°W). There is inflow to the region from the west (Amchitka Pass and Bowers Ridge) and from the south via Amukta Pass. The continental slope and adjacent shelf in this region has been extensively studied in recent decades, and has been classified (Kinder et al. 1975, 1980; Kinder and Schumacher 1981; Royer and Emery 1984) as an area of frequent eddies.

The annual cycle in this region is dominated by seasonal rather than interannual variability (see Figs. 5 and 6), and is illustrated in Fig. 15. Here the upper-layer depth-averaged current is drawn at bimonthly intervals during model year 41. For clarity the Alaskan Stream, south of the Aleutian Island chain, has been suppressed and the average wind stress vector for the subregion inserted. The year begins with a strong flow along the northern flank of the Aleutian Islands. A hydrographic survey and satellite-tracked buoys in March and April of 1988 (Reed and Stabeno 1989) show a coherent cyclonic circulation through the region south of the Pribilof Islands, consonant with the model simulation. This flow is maintained until May when it begins to move offshore. By July a well-defined countercurrent has been established, flowing to the west and entraining the inflow from the Pacific at Amukta Pass. The shear zone between the nearshore current and the normal counterclockwise basin flow, that has been displaced offshore, is marked by a string of anticyclonic eddylike features. An anticyclonic eddy of similar scale and location is seen in a satellite IR image from 23 August 1980 (Paluszkiewicz and Niebauer 1984). In October (not shown) the countercurrent begins to weaken and move offshore and, in a transition not resolved by the bimonthly images, the eastward coastal current has become reestablished by November. A westward nearshore flow is seen in the summer dynamic topography of Sayles et al. (1979), and the intermittent signature of water properties associated with inflow through Amukta Pass (Reed 1991) might be associated with the seasonal reversals evident in Fig. 15.

d. Northern Bering basin

As was the case in the southeastern portion of the basin, there is a regular seasonal cycle in response to the monthly winds. In Fig. 16 the upper-layer circulation for model year 41 is shown. In Fig. 7 a seasonal reversal of the transport through a north–south section at the northern head of the model basin was noted. The mechanism for this, and other features of the Bering slope current (Kinder et al. 1975), is seen to be associated with the westward propagation of eddies that form near the slope. These eddies seem to originate preferentially in embayments of the slope, for example those near 57°–58°N, 59°–60°N. The year begins with the slope current lying close to the model boundary. By May or June anticyclonic eddies in these embayments begin to displace the northwestward flow offshore. The eddies themselves propagate to the west to be replaced, near the end of the year, by weaker cyclonic eddies that restore the normal slope current abruptly between November and December. The motion of the eddies formed near 59.5°N is illustrated more clearly in the space–time diagram of Fig. 17. Here the vorticity $(v_x - u_y)$ is contoured in time for the transect CC of Fig. 12. The westward movement of the eddies that form near 179°W is evident. Their propagation speed

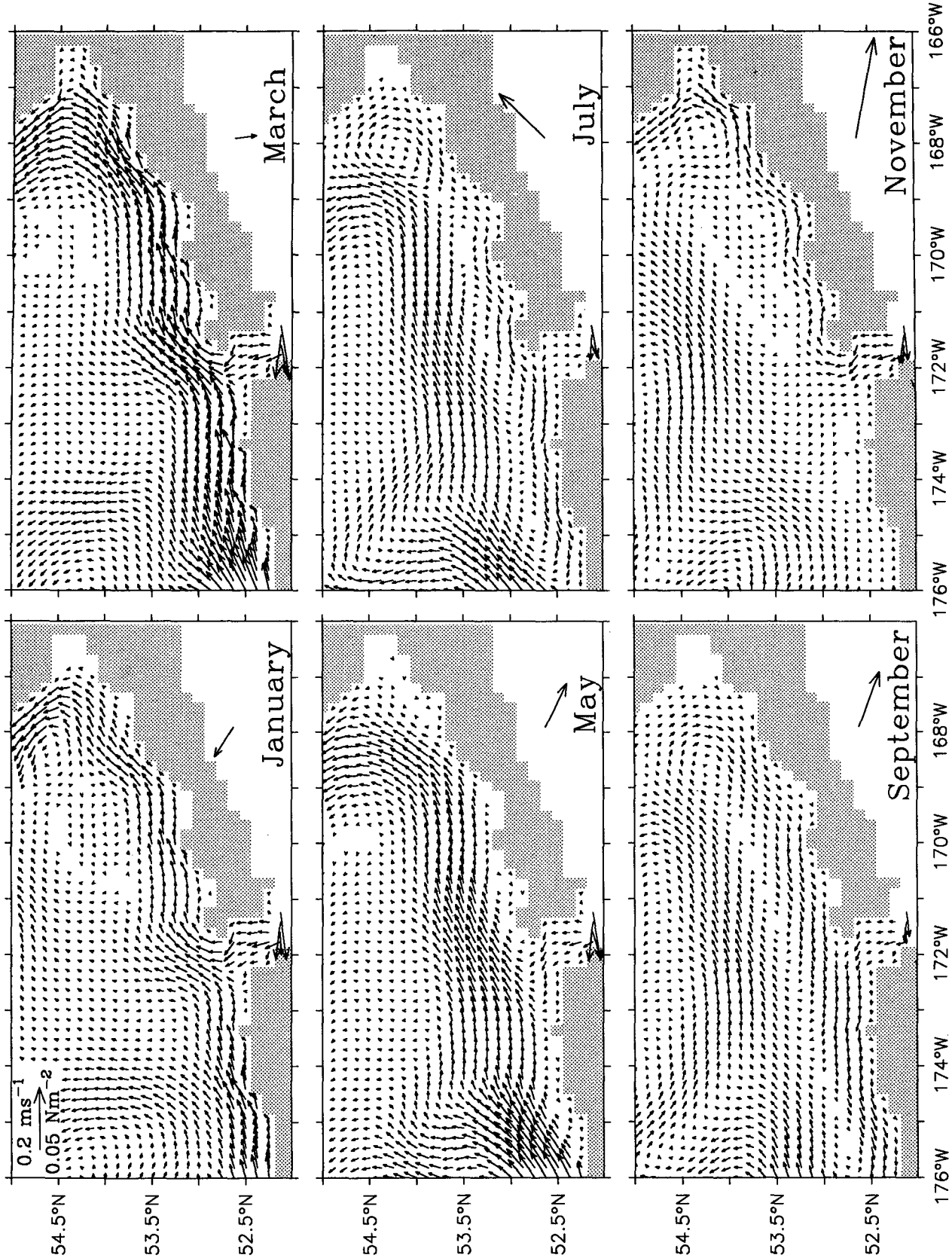

FIG. 15. Upper-layer circulation in the southeastern corner of the Bering basin during model year 41. The reversal in the coastal current, seen in these bimonthly images, is repeated annually throughout the decade, and the shear zone may be a source for the eddies that are frequently observed in this region.

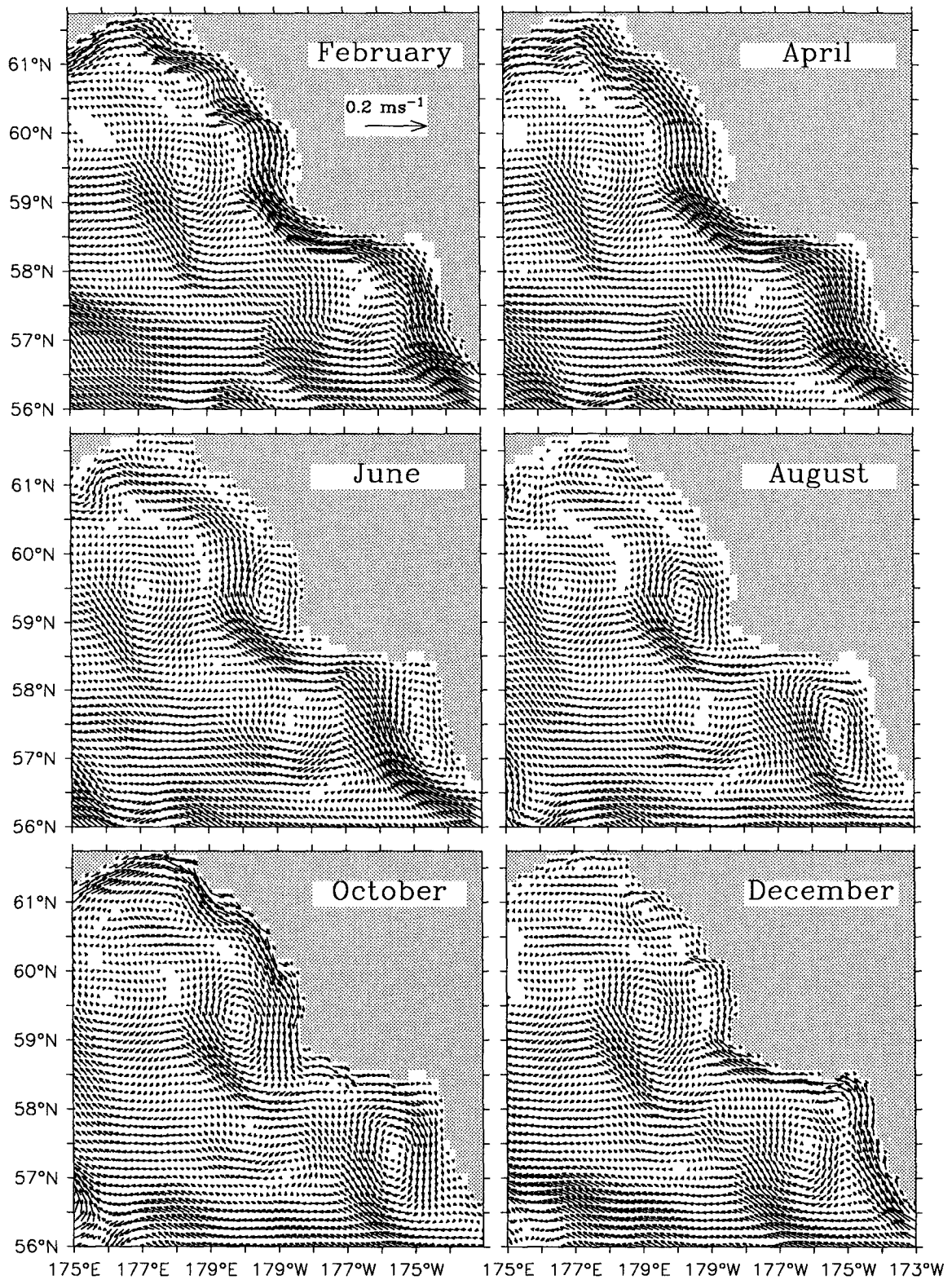

FIG. 16. Upper-layer circulation in the northern portion of the Bering basin during model year 41. Bimonthly images are drawn for the region delineated in Fig. 12. The Bering slope current reverses annually as eddies form and propagate westward from embayments in the continental slope.

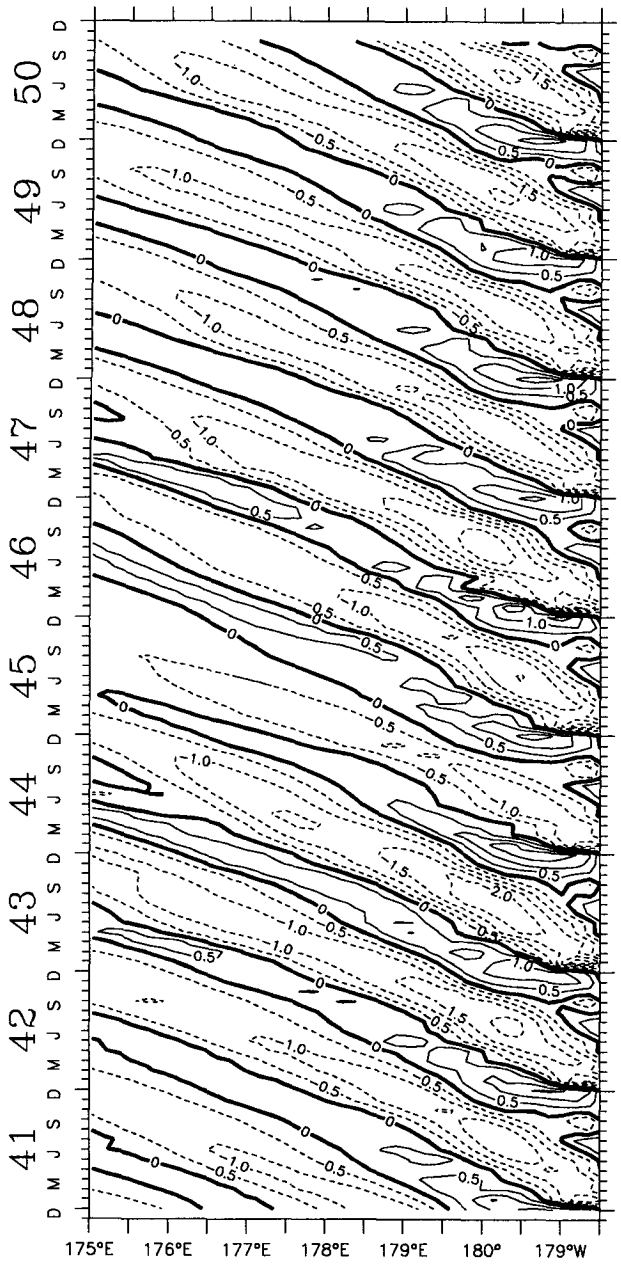

FIG. 17. Time evolution of vorticity along an east-west transect at 59.5°N (CC in Fig. 12). Westward propagation of eddies that form near the slope of the Bering shelf is evident.

of 0.6 km day^{-1} is similar to the group speed of Rossby waves with scales of order 100 km at these latitudes. One of the simulated drifters in Fig. 11 moves westward in such an eddy, and a number of actual satellite-tracked buoys have followed similar paths (P. Stabeno 1993, personal communication). Strong variability in the northern Bering Sea basin is evident in the statistics of Stabeno and Reed (1994), but the temporal sampling is insufficient to confirm a seasonally reversing Bering slope current. Eddylike features and counter-flows are evident in the dynamic topography of Kinder et al. (1975), and these authors present an interpretation based on planetary waves of annual periodicity. More recently Schumacher and Reed (1992) report complex patterns in CTD surveys, but their moored current meter observations on the slope suggest brief and intermittent rather than seasonal reversals.

e. Kamchatka Current

When forced by the Alaskan Stream and the Hellerman and Rosenstein (1983) wind climatology the model predicts outflow from the Bering Sea basin through Kamchatka Strait only. As seen in section E of Fig. 7, the total transport varies seasonally between 8 and 13 Sv with the peak outflow occurring in February. The origins of the Kamchatka Current as a counterclockwise boundary current lie in the vicinity of 165°E. Further east, while there is continuity in winter with the Bering slope current, the flow along the northernmost portion of the model domain reverses in summer and fall. A further contribution to the Kamchatka Current comes from a broad westward drift across the basin. The Kamchatka Current in the model is narrow, even away from the constriction of Kamchatka Strait. The annual average axis is drawn as the curve KK in Fig. 12, together with a zonal range based on twice the standard deviation. The Kamchatka current is quite steady (Fig. 6) and no large meanders, such as seen in the Alaskan Stream, are observed within the Bering Sea. Satellite-tracked buoys (Stabeno and Reed 1994) have revealed meandering of the Kamchatka Current and eddy-shedding in this region. South of Kamchatka Strait the current flows offshore of a series of embayments, the northernmost of which is Kamchatskiy Bay. Figure 6 shows the greater variability associated with anticyclonic eddies that form in these embayments. These resemble the anticyclonic eddy reported in infrared imagery by Solomon and Ahlnäs (1978), and the pockets of high variability evident in the satellite-tracked buoy statistics of Stabeno and Reed (1994). Model eddies pinched off the Alaskan Stream, entering the Kamchatka Current in this region, tend to rotate counterclockwise, as do eddies entrained north of the Komandorski Islands.

6. Conclusions

The results produced by the Navy model (Hurlburt et al. 1992), when forced by the climatological winds and a steady throughput of the Alaskan Stream, are in general agreement with prior understanding of the circulation in the Bering Sea basin. The Alaskan Stream remains steady and lies close to the Aleutian Island chain until about 175°E where it separates. Strong meanders develop intermittently that may shed eddies that persist for many months, imposing an interannual variability on the main inflow to the Bering via Near

Strait. The circulation within the Bering Sea basin is generally cyclonic, complex in spatial structure, and nonstationary. An intense eddying region west of Bowers Ridge is a quasipermanent feature. An eastward flow along the northern flank of the Aleutian Island chain is augmented by inflow through other passes before turning northward and westward across the basin. A narrow Kamchatka Current is formed along the western boundary, beginning about 165°E. On exiting the Bering Sea via Kamchatka Strait the current induces eddies in embayments of the Kamchatka Peninsula. A portion of the current exits the outflow port, while the remainder flows eastward along the southern boundary of the model. The outflowing portion mimics the Oyashio Current while the remainder, recirculating into the Alaskan Stream as it moves east, represents the southern limb of the western subarctic gyre.

The 1/8° resolution and multiyear integration allow previously unidentified features, such as the seasonal reversals of flow in the northern and southeastern portions of the Bering Sea basin, to be identified. Model statistics for eddy variability are available for comparison with satellite altimetry and satellite buoy-tracking in complementary studies of the region.

Satellite-tracked buoy statistics, presented by Stabeno and Reed (1994), support the general circulation pattern produced by the model when forced by a steady Alaskan Stream and periodic climatological wind forcing. Some specifics such as the intense eddy region west of Bowers Ridge and the zonal nature of the inflow through Near Strait are confirmed by the observations. The model results presented here do not reproduce the meanders in the Kamchatka Current reported by Stabeno and Reed (1994) within the Bering Sea. Neither does the range of interannual variability in the flow through Near Strait fully explain the anomalous circulation pattern described by Stabeno and Reed (1992) in which inflow to the Bering was drastically curtailed during 1990 and 1991.

Other features, such as the seasonal reversals in the northern and southeastern portions of the Bering Sea basin, are neither endorsed nor contradicted by the temporally sparse observational database. While planetary waves of annual periodicity were invoked by Kinder et al. (1975) to explain dynamic topographic features along the Bering Sea slope, seasonal reversals of the flow were not observed in the current meter records of Schumacher and Reed (1992).

Preliminary results from model runs forced by ECMWF (European Centre for Medium-Range Weather Forecasts) winds for 1985–1992 suggest that the extended periodic forcing in the simulation reported here may overemphasize the seasonal response. Flow reversals still occur in the southeast and north of the basin but interannual variability is greatly enhanced. The new results confirm the zonal nature of the inflow through Near Strait. Episodes of reduced inflow to the Bering via Near Strait (as little as 1.6 Sv) and weakening of the outflow through Kamchatka Strait show promise of simulating the observations of Stabeno and Reed (1992) and Verkhunov and Tkachenko (1992). Available as 12-hourly gridded fields the ECMWF (or NMC) winds will allow the role of temporal smoothing in the forcing to be investigated in the manner of Large et al. (1991).

Acknowledgments. This paper is dedicated to the memory of L. K. Coachman and J. D. Thompson. They were pioneers in the Bering Sea and numerical studies, respectively. It is a contribution to the Fisheries–Oceanography Coordinated Investigations (FOCI) and to the Joint Institute for the Study of the Atmosphere and Ocean (JISAO). It is sponsored by the Coastal Fisheries Ecosystem Project of NOAA's Coastal Ocean Program. We thank P. Stabeno for her interest in these numerical experiments. The FERRET system, developed at NOAA/PMEL/OCRD was used to analyze the model output and produce the graphics. The work by Hurlburt and Wallcraft was supported by the 6.1 Eddy-resolving Global Ocean Model project sponsored by the Office of Naval Research (program element 61153N; William Moseley, program manager) and by the 6.2 Global Ocean Prediction System Project sponsored by the Office of Naval Technology (program element number 62435N) as part of the Naval Ocean Modeling and Prediction Program (Robert Peloquin, program manager).

REFERENCES

Abramowitz, M., and I. A. Stegun, 1964: *Handbook of Mathematical Functions. Appl. Math. Series.* Vol. 55, National Bureau of Standards, 1046 pp.

Barnes, C. A., and T. G. Thompson, 1938: Physical and chemical investigations in the Bering Sea and portions of the North Pacific Ocean. *Univ. Wash. Publ. Oceanogr.*, **3,** 35–79, A1–A164.

Bond, N. E., J. E. Overland, and P. Turet, 1994: Spatial and temporal characteristics of the wind forcing of the Bering Sea. *J. Climate,* **7,** in press.

Cummins, P. F., 1989: A quasi-geostrophic circulation model of the northeast Pacific. Part II: Effects of topography and seasonal forcing. *J. Phys. Oceanogr.*, **19,** 1649–1668.

——, and H. J. Freeland, 1993: Observations and modeling of wind-driven currents in the Northeast Pacific. *J. Phys. Oceanogr.*, **23,** 488–502.

Defant, A., 1936: The troposphere. *Scientific Results of the German Atlantic Expedition of the Research Vessel "Meteor" 1925–27,* Vol 6 (Part 1), English translation edited by W. J. Emery, U.S. Dept. of Commerce, National Technical Information Service.

Favorite, F., 1974: Flow into the Bering Sea through Aleutian Island passes. *Oceanography of the Bering Sea with Emphasis on Renewable Resources,* D. W. Hood and E. J. Kelly, Eds., University of Alaska, Occasional Publication No. 2, 3–37.

Hellerman, S., and M. Rosenstein, 1983: Normal monthly wind stress over the world ocean with error estimates. *J. Phys. Oceanogr.*, **13,** 1093–1104.

Hughes, F. W., L. K. Coachman, and K. Aagaard, 1974: Circulation, transport and water exchange in the western Bering Sea. *Oceanography of the Bering Sea,* D. W. Hood and J. J. Kelly, Eds., Institute of Marine Science, University of Alaska, 59–98.

Hurlburt, H. E., and J. D. Thompson, 1980: A numerical study of Loop Current intrusions and eddy shedding. *J. Phys. Oceanogr.*, **10,** 1611–1651.

——, A. J. Wallcraft, Z. Sirkes, and E. J. Metzger, 1992: Modelling of the global and Pacific Oceans: On the path to eddy-resolving ocean prediction. *Oceanography,* **5,** 9–18.

Kinder, T. H., and J. D. Schumacher, 1981: Circulation over the continental shelf of the southeastern Bering Sea. *The Bering Sea Shelf, Oceanography and Resources,* D. W. Hood, Ed., Dept. of Commerce, NOAA, 53–93.

——, L. K. Coachman, and J. A. Galt, 1975: The Bering slope current system. *J. Phys. Oceanogr.,* **5,** 231–244.

——, J. D. Schumacher, and D. V. Hansen, 1980: Observation of a baroclinic eddy: An example of mesoscale variability in the Bering Sea. *J. Phys. Oceanogr.,* **10,** 1228–1245.

Kundu, P. K., 1976: Ekman veering observed near the ocean bottom. *J. Phys. Oceanogr.,* **6,** 238–242.

Large, W. G., W. R. Holland, and J. C. Evans, 1991: Quasi-geostrophic ocean response to real wind forcing: The effects of temporal forcing. *J. Phys. Oceanogr.,* **21,** 998–1017.

Levitus, S., 1982: *Climatological Atlas of the World Ocean.* NOAA Prof. Paper 13, Geophysical Fluid Dynamics Laboratory, Princeton, NJ, 173 pp.

NOAA, 1991: *NOAA's Coastal Ocean Program, Prospectus for Fiscal Years 1993–97.* U.S. Department of Commerce, 163 pp.

Orlanski, I., 1976: A simple boundary condition for unbounded hyperbolic flows. *J. Comput. Phys.,* **21,** 251–269.

Paluszkiewicz, T., and H. J. Niebauer, 1984: Satellite observations of circulation in the eastern Bering Sea. *J. Geophys. Res.,* **89,** 3663–3678.

Reed, R. K., 1984: Flow of the Alaskan Stream and its variations. *Deep-Sea Res.,* **31,** 369–386.

——, 1990: A year-long observation of water exchange between the North Pacific and the Bering Sea. *Limnol. Oceanogr.,* **35,** 1604–1609.

——, 1991: Circulation and water properties in the central Bering Sea during OCSEAP studies, Fall 1989–Fall 1990. NOAA Tech. Rep. ERL 446-PMEL 41, NOAA Environmental Research Laboratories, Boulder CO, 13 pp.

——, and P. J. Stabeno, 1989: Circulation and property distributions in the central Bering Sea, Spring 1988. NOAA Tech. Rep. ERL 439-PMEL 39, NOAA Environmental Research Laboratories, Boulder CO, 13 pp.

——, A. V. Verkhunov, G. V. Khen, E. D. Cokelet, J. E. Overland, and T. E. Whitledge, 1992: Recent U.S.–U.S.S.R. cruise in the Bering Sea. *Eos,* **73,** 184.

Reid, J. L., 1973: *Northwest Pacific Ocean Waters in Winter.* Johns Hopkins University Press, 96 pp.

Royer, T. C., and W. J. Emery, 1984: Circulation in the Bering Sea, 1982–83, based on satellite-tracked drifter observations. *J. Phys. Oceanogr.,* **14,** 1914–1920.

Sayles, M. A., K. Aagaard, and L. K. Coachman, 1979: *Oceanographic Atlas of the Bering Sea Basin.* University of Washington Press, 158 pp.

Schumacher, J. D., and R. K. Reed, 1992: Characteristics of currents over the continental slope of the Eastern Bering Sea. *J. Geophys. Res.,* **97,** 9423–9433.

——, C. A. Pearson, and J. E. Overland, 1982: On exchange of water between the Gulf of Alaska and the Bering Sea through Unimak Pass. *J. Geophys. Res.,* **87,** 5785–5795.

Shapiro, R., 1970: Smoothing, filtering and boundary effects. *Rev. Geophys. Space Phys.,* **8,** 359–387.

Solomon, H., and K. Ahlnäs, 1978: Eddies in the Kamchatka Current. *Deep-Sea Res.,* **25,** 403–410.

Stabeno, P. J., and R. K. Reed, 1991: Recent Lagrangian measurements along the Alaskan Stream. *Deep-Sea Res.,* **38,** 289–296.

——, and ——, 1992: A major circulation anomaly in the western Bering Sea. *Geophys. Res. Lett.,* **19,** 1671–1674.

——, and ——, 1994: Circulation in the Bering Sea observed by satellite-tracked drifters: 1986–1993. *J. Phys. Oceanogr.,* **24,** 848–854.

Takenouti, A. Y., and K. Ohtani, 1974: Currents and water masses in the Bering Sea: A review of Japanese work. *Oceanography of the Bering Sea,* D. W. Hood and J. J. Kelly, Eds., Institute of Marine Science, University of Alaska, 39–57.

Thompson, J. D., and W. J. Schmitz, 1989: A limited area model of the Gulf Stream System: Initial design experiments and model-data intercomparison. *J. Phys. Oceanogr.,* **19,** 791–814.

Thomson, R. E., 1972: On the Alaskan Stream. *J. Phys. Oceanogr.,* **2,** 363–371.

Verkhunov, K. H., and Y. Y. Tkachenko, 1992: Recent observations of variability in the western Bering Sea current system. *J. Geophys. Res.,* **97,** 14 369–14 376.

Wallcraft, A. J., 1991: The Navy Layered Ocean Model Users' Guide. NOARL Report 35, Stennis Space Center, MS, 21 pp.